SECRET

UNCLASSIFIED

NAA-SR-9407
COPY 117 OF 225
50 PAGES
SERIES A

MASTER

SNAP 2 REACTOR ADVANCED PERFORMANCE CAPABILITY STUDY

(Title Unclassified)

AEC Research and Development Report

RESTRICTED DATA

ATOMICS INTERNATIONAL
A DIVISION OF NORTH AMERICAN AVIATION, INC.

UNCLASSIFIED

SECRET

DISCLAIMER

LEGAL NOTICE

Printed in USA **Price $1.05** **Available from the**

U. S. Atomic Energy Commission
Technical Information Extension,
P. O. Box 1001
Oak Ridge, Tennessee.

Please direct to the same address inquiries covering the procurement of other classified AEC reports.

~~SECRET~~
~~UNCLASSIFIED~~

NAA-SR-9407
SNAP REACTOR,
SNAP PROGRAM
M-3679 (34th Ed.)

SNAP 2 REACTOR ADVANCED PERFORMANCE CAPABILITY STUDY

(Title Unclassified)

By

J. D. GYLFE
J. K. BALKWILL
W. A. FLYNN
D. J. McGOFF
M. E. NATHAN
J. SUSNIR
J. D. WATROUS
J. D. WILDE, JR.

ATOMICS INTERNATIONAL

A DIVISION OF NORTH AMERICAN AVIATION, INC.
P.O. BOX 309 CANOGA PARK, CALIFORNIA

~~UNCLASSIFIED~~
~~SECRET~~

CONTRACT: AT(11-1)-GEN-8
ISSUED: JUNE 2, 1964

GG

DISTRIBUTION

SYSTEMS FOR NUCLEAR AUXILIARY POWER (SNAP)-REACTOR SNAP PROGRAM M-3679 (34th Ed.)

	Copy No
Aerojet-General Corporation (NASA)	1
Aerojet-General Nucleonics	2
Aeronautical Systems Division	3-4
Aerospace Corporation	5
Aerospace Test Wing (AFSC)	6
Air Force Weapons Laboratory	7-8
AiResearch Manufacturing Company, Phoenix	9
Army Ballistic Research Laboratories	10
Army Materials Research Agency	11
Army Missile Command	12
Army Nuclear Defense Laboratory	13
ARO, Inc.	14
Air University Library	15
Argonne National Laboratory	16
Army Combat Developments Command	17
Astropower, Inc.	18
Avco Corporation	19
Battelle Memorial Institute	20
Bendix Corporation (AF)	21
Brookhaven National Laboratory	22
Bureau of Naval Weapons	23-24
Bureau of Ships	25-26
Bureau of Yards and Docks	27
California Patent Group	28
Central Intelligence Agency	29
Chicago Patent Group	30
Defense Atomic Support Agency, Sandia	31
Department of the Army	32
Director of Defense Research and Engineering (OAP)	33
Edgerton, Germeshausen and Grier, Inc., Goleta	34
Foreign Technology Division (AFSC)	35
General Atomic Division	36
General Dynamics/Astronautics (AF)	37
General Dynamics/Fort Worth	38
General Electric Company, Cincinnati	39
General Electric Company (FPD)	40-41
General Electric Company (MSVD)	42
General Electric Company, Richland	43-44
General Electric Company, San Jose	45
General Electric Company, San Jose (AF)	46
General Technologies Corporation	47
Institute for Defense Analysis	48
Ion Physics Corporation	49
Jet Propulsion Laboratory	50-51
Johns Hopkins University (APL)	52
Lockheed-Georgia Company	53
Lockheed-Missiles and Space Company	54
Los Alamos Scientific Laboratory	55
Martin-Marietta Corporation, Denver	56
Monsanto Dayton Laboratory	57
NASA Ames Research Center	58
NASA Goddard Space Flight Center	59-60
NASA Langley Research Center	61
NASA Lewis Research Center	62-65
NASA Manned Spacecraft Center	66
NASA Marshall Space Flight Center	67
NASA Scientific and Technical Information Facility	68-70
National Aeronautics and Space Administration, Washington	71
NASA Western Operations Office	72
Naval Air Development Center	73
Naval Ordnance Laboratory	74-75
Naval Postgraduate School	76
Naval Radiological Defense Laboratory	77
Naval Research Laboratory	78-79
Naval Underwater Ordnance Station	80
Navy Marine Engineering Laboratory	81
New York Operations Office	82
New York Operations Office, Canel Project Office	83
North American Aviation, Inc., Downey	84
Nuclear Metals, Inc.	85
Office of Naval Research	86-87
Office of the Assistant General Counsel for Patents (AEC)	88
Office of the Chief of Engineers	89
Office of the Chief of Naval Operations	90-92
Office of the Chief of Naval Operations (OP-03EG)	93-94
Office of the Chief of Transportation	95
Phillips Petroleum Company (NRTS)	96-99
Pratt and Whitney Aircraft Division	100
Pratt and Whitney Aircraft Division (NASA)	101
Rand Corporation	102
Republic Aviation Corporation	103
Sandia Corporation	104
School of Aerospace Medicine	105
Union Carbide Corporation (ORNL)	106-113
USAF Headquarters	114
University of California, Livermore	115
Westinghouse Electric Corporation (NASA)	116
Division of Technical Information Extension	117-156
AI Library (Includes 2 copies to CPAO, 2 copies to AEC, Washington, 2 copies to COO)	157-225

CONTENTS

TABLES

FIGURES

FIGURES

BLANK

I. INTRODUCTION

This report presents the results of a study which was performed to determine the maximum power and temperature capability of the SNAP 2 reactor concept, based on minimal extrapolation of current technology. The present SNAP 2 reactor design, which is described briefly in Section III, is being developed as the nuclear heat source for the SNAP 2 Compact Power Unit which utilizes a mercury-Rankine cycle to generate 3.5 kw electrical power. This system requires a reactor capable of producing 55 kw thermal power which is transferred to a NaK coolant loop at a maximum coolant temperature of 1235°F.

Prior to freezing the design for the SNAP 2 reactor system, it is considered necessary to re-evaluate the performance margins available in the present design and to determine the nature and extent of the design modifications required to increase both the power and the maximum coolant temperature capability. This information is needed to estimate the reliability of the reactor at its present design point and to incorporate those features which would permit operation over a wide range of operating conditions.

Although studies of this general nature were performed when the SNAP 10A/2 reactor was conceived, progress in the development and testing of SNAP fuel elements, improved nuclear data and analytical techniques, and operational data from the SNAP 2 Developmental Reactor require a timely reappraisal of this subject.

On the basis of previous analyses and operating experience, it is known that the most fundamental limitation on reactor power level and temperature for long-term operation is the loss of reactivity due to excessive hydrogen leakage from the zirconium hydride-uranium alloy fuel-moderator elements. As the temperature of the reactor core is increased, the hydrogen dissociation pressure increases, as does the permeation rate through the ceramic diffusion barrier which is applied to the inside of the fuel-moderator cladding. Since the core is inherently undermoderated, any loss of hydrogen moderator results in a loss of reactivity. This long-term reactivity change is compensated by the gradual burnout of samarium oxide prepoison which is incorporated in the elements and by inward rotation of the control drums.

At the present SNAP 2 operating conditions, the total reactivity loss due to hydrogen leakage is relatively small compared to the total cold, clean reactivity requirements. Due to the exponential relationship between hydrogen dissociation pressure, hydrogen permeation rate, and fuel temperature, however, the importance of hydrogen leakage increases rapidly at higher reactor power levels and/or coolant temperatures. Fortunately, several design variables can be adjusted to compensate for these effects. The most important of these design variables are:

a) Increased Reflector Thickness — The nominal thickness of the beryllium reflector for the present SNAP 2 design is ≈2.3 in. whereas an essentially "infinite" reflector would be ~10 in. thick. Thus, the initial reactivity of the reflected reactor and the control drum worth can be increased substantially by increasing the radial-reflector thickness. However, since the reactor must be subcritical with two of the four control drums fully rotated inward, a definite limit on reflector thickness exists for a given core composition and geometry.

b) Reduced N_H — The hydrogen dissociation pressure for zirconium hydride is strongly dependent on the H/Zr atom ratio. By reducing this ratio (and hence the initial hydrogen concentration, N_H) the hydrogen loss rate can be reduced, at the expense of initial reactivity. This reduction of initial reactivity must be compensated by increasing the reflector thickness.

c) Decreased Fuel-Moderator Element Diameter — The maximum and average temperature of the cylindrical ZrH-U alloy fuel moderator elements can be reduced by decreasing the element diameter. While this modification reduces the hydrogen pressure within the element, the available area for hydrogen permeation is increased. Therefore, a theoretically optimum diameter exists for a given set of operating conditions, with a larger number of small diameter elements being preferable for higher power density cores.

d) Increased U-235 Loading — Increasing the U-235 loading will provide a gain in initial reactivity, but since the SNAP 2 core is undermoderated and since the additional fuel atoms must displace zirconium (and thus hydrogen) atoms in the alloy fuel moderator elements, the net gain for extending long-term operation is small.

The core size is another design variable which would obviously affect the reactor power capability. Due to the substantial amount of critical experiment and operational data available for the present SNAP 2 core designs, however, the design variables considered in the present study were limited to the first two items discussed above; i. e., reflector thickness and hydrogen density.

The reactor power level and coolant outlet temperature were varied parametrically over a range up to 200 kwt and 1350°F respectively. The coolant temperature rise through the core was held constant at 200°F, since this value has been shown to be near optimum for various power conversion systems over a wide range of power levels.

The analysis was conducted in three major areas: core heat transfer, fuel element performance, and nuclear analysis. The basic assumptions, methods, and results of these tasks are described in Sections IV through VI and the conclusions of the study are included in the summary.

BLANK

II. SUMMARY AND CONCLUSIONS

The reactivity limits and design modifications required to achieve high power and elevated temperature operation of the SNAP 2 reactor concept have been investigated and defined. Core heat transfer analyses established fuel element temperatures for thermal power levels ranging from 53 to 200 kw and coolant outlet temperatures from 1200 to 1350°F. Maximum fuel temperatures along the centerline of the hottest element ranged from 1275°F at 53 kw, 1200°F NaK outlet temperature to ~1690°F at 200 kw, 1300°F NaK outlet temperature. Maximum clad and hydrogen barrier temperatures for corresponding operating conditions ranged from ~1230 to 1440°F.

Analytical methods for estimating hydrogen leakage from the fuel elements at advanced operating conditions were developed to account for the temperature distributions within the fuel and over the clad surface, and hydrogen redistribution within the fuel. Leakage coefficients were developed to account for leakage through the blend and through the coated clad walls. These leakage coefficients were obtained from out-of-pile leak rate measurements on 50 production elements assembled for the SNAP 10A FS-1 core. Hydrogen leakage rates were then computed for the range of operating conditions studied and for initial hydrogen concentrations (N_H) ranging from 6.0×10^{22} to 6.5×10^{22} atoms/cm^3.

Clad strain due to hydrogen pressure buildup at the higher operating conditions was investigated and found acceptable. Potential fuel swelling problems were also investigated. Based on conservative application of existing data, it is concluded that radial growth would not be sufficient to cause contact between the fuel-moderator rod and the clad barrier, even at the 200 kwt/1350°F operating conditions. Due to the lack of adequate expansion space at the hot operating conditions, axial fuel swelling at power levels above ~150 kwt could present a problem with the present fuel element design. If future in-pile tests and more rigorous analyses indicate that a problem exists, additional space can be provided to accommodate axial expansion.

The nuclear analyses established reactivity requirements to compensate for temperature and power defects, xenon buildup, hydrogen redistribution, fuel depletion, fission product buildup, hydrogen leakage and samarium buildup and burnout over the complete range of power levels and coolant temperatures

studied. Total cold, clean reactivity requirements were found to vary from approximately $3.00 to $8.00.

The initial hydrogen density and reflector thickness were varied for each operating point to determine the minimum weight and size reflector which would provide sufficient reactivity and control for one year operation while maintaining a cold shutdown margin of at least 50¢ with two control drums rotated full in. Shield weight increments were also calculated, based on maintaining a constant vehicle dose rate and separation distance.

The most significant results obtained from this study are summarized on Figure 1. This figure illustrates the combinations of reactor power level and coolant outlet temperature which can be achieved with the current reference design, by increasing the reflector weight in 10 lb increments up to 40 lb and by adjusting the hydrogen density (N_H) in the core. These results show that the present SNAP 2 reactor design concept has a reactivity margin sufficient to sustain operations for one year at ~250% of design power at the design coolant temperatures or at 100°F higher coolant temperatures at the design power level.

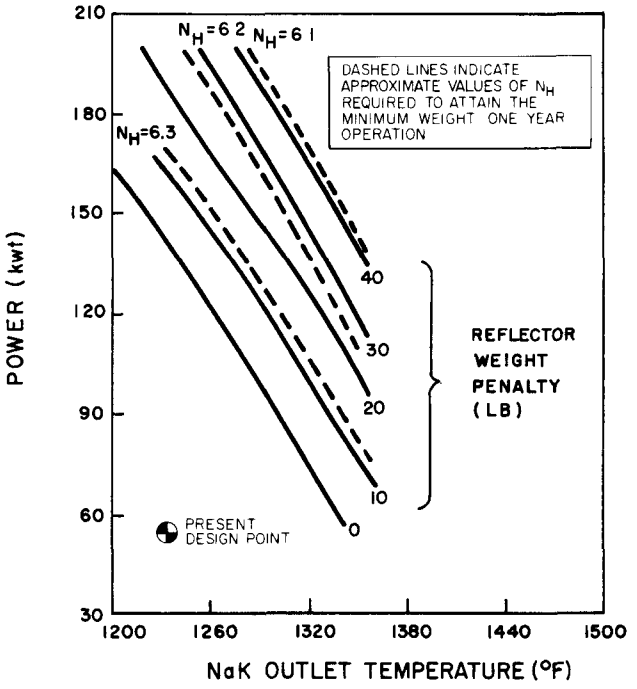

1-22-64 7635-0037

Figure 1. Minimum Weight Penalties vs Power and Temperature

Also, the present SNAP 2 reflector and control drum design can accommodate ~20 additional pounds of beryllium shims with relatively minor redesign. With this modification, and by dropping the N_H to ~6.25 x 10^{22} atoms/cm^3, the reactor should thus be capable of one year operation at ~140 kwt with a maximum coolant outlet temperature of 1300°F or ~185 kwt at 1235°F.

By reducing the N_H to ~6.1 x 10^{22} and redesigning the reflector block and control drums to permit an additional increase in reflector weight (to 40 lb), the power level or coolant temperature could be raised approximately another 40 kwt or 50°F respectively. Subsequent studies, however, have indicated that this last extrapolation from the reference design would be less desirable than modification of the core design to use a larger number of smaller diameter elements.

The total weight change (reflector plus shield) required to increase the power and/or coolant temperature and maintain a constant fast neutron flux at an arbitrarily fixed dose plane is shown in Figure 2. However, both the reactor-payload separation distance and the shadow shield angle would probably change for the higher power applications and the incremental shield weights shown are thus somewhat academic.

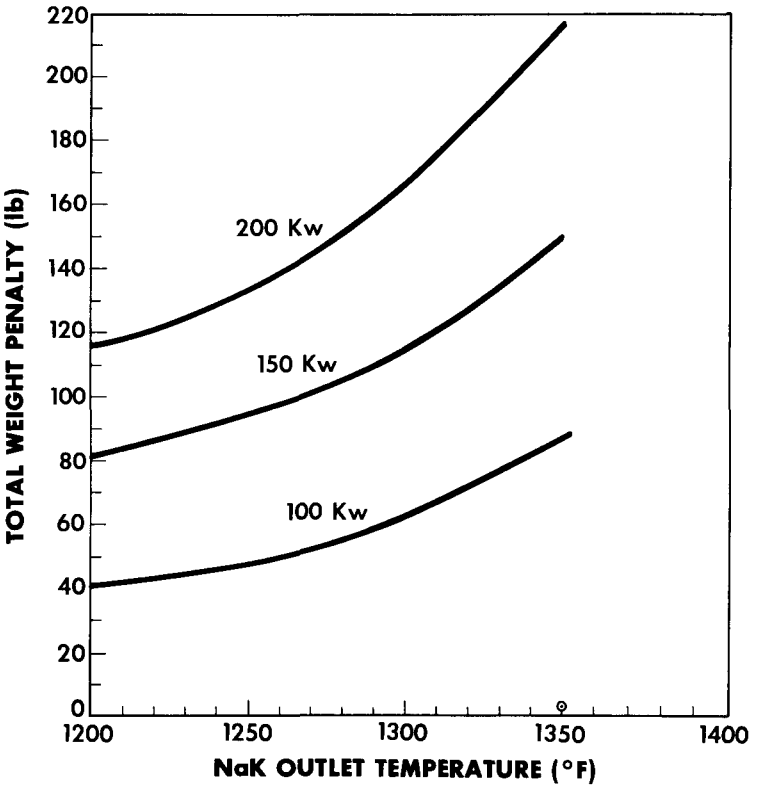

Figure 2. Total Weight Penalty vs NaK Outlet Temperature (Shield Plus Reflector)

10-8-63 7622-0066

BLANK

III. DESCRIPTION

An artist's concept of the SNAP 2 reactor, reflector, and shield assembly is shown on Figure 3 and a summary of the major design and performance characteristics is presented in Table 1.

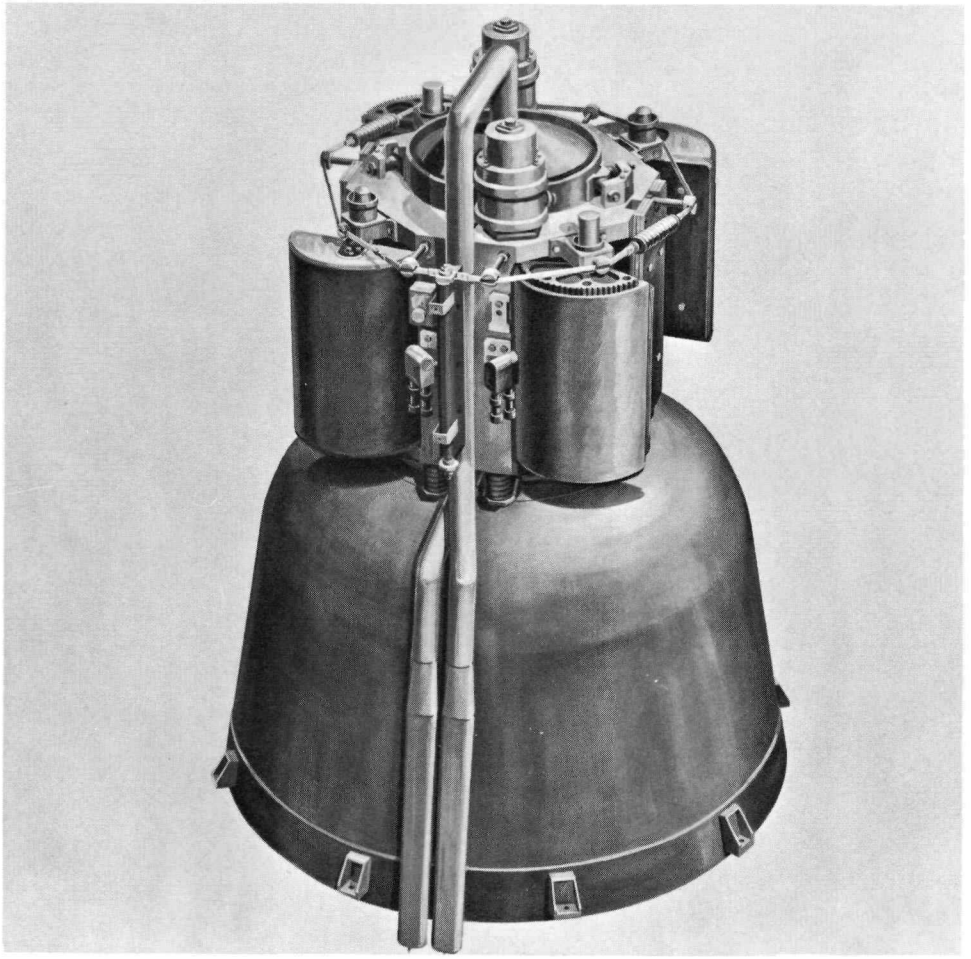

8-21-63 7622-0025

Figure 3. Artist's Concept of SNAP 2 Reactor, Reflector and Shield Assembly

The reactor assembly consists of a thin-walled, stainless steel vessel assembly, inlet and outlet NaK lines, grid plates, fuel-moderator elements, internal reflectors and the core support structure, assembled as shown in the cutaway view, Figure 4. The reactor core consists of 37 fuel-moderator elements arranged in a close-packed hexagonal array. The internal reflectors fill the spaces between the hexagonal core and the circular vessel.

TABLE 1

SUMMARY OF DESIGN AND PERFORMANCE REQUIREMENTS AND CHARACTERISTICS SNAP 2 REACTOR SUBSYSTEM

I	*Performance Requirements*		
	Reactor thermal power (kw)		
	to NaK	53	
	Heat loss to space	2	
	Total	55	
	Coolant outlet temperature (°F)		
	Max	1235	
	Min	1185	
	Coolant inlet temperature (°F)		
	Max	1015	
	Min	963	
	Nominal coolant flow rate (lb/min)	70	
	Minimum operating lifetime (yr) in space Environment	1	
	Maximum launch acceleration (g's)		
	Axial	+7 6 -2 5	
	Lateral and normal	±1 0	
	Maximum launch vibration		
	Longitudinal	g's / frequency (cps)	
		1/2 in D A / 5 - 12	
		3 5 / 12 - 400	
		7 5 / 400 - 3000	
	Lateral and normal	g's / frequency (cps)	
		1/2 in D A / 5 - 10	
		2 5 / 10 - 250	
		5 0 / 250 - 400	
		7 5 / 400 - 3000	
	Subsystem weight objective (not including electronic equipment)	630 lb	
	Fast neutron dose rate at CPU/AGENA mating plane (nvt/yr)	5×10^{12}	
	Gamma dose rate at CPU/AGENA mating plane r/yr	10^7	
II	*Reactor Design Characteristics*		
	Core		
	Equivalent diameter (in)	8 10	
	Active height (in)	12 25	
	Fuel	U235 (enriched)	
	Moderator	Zirconium hydride	
	Number of fuel-moderator elements	37	
	Fuel element diameter (in)	1 25	
	Cladding	Hastelloy N	
	Permeation barrier	AI 'D'	
	Fuel-moderator alloy composition (wt %)	U	
	Uranium	10	
	Carbon	0 1	
	Zirconium hydride	90	
	Effective hydrogen density (atoms/cm^3 x 10-22)	6 35	
	Prepoison material	Samarium	
	Internal reflector material	clad BeO	
	Grid plate material	42% Ni-Fe Low Exp Alloy	
	Vessel		
	Material	SS 321	
	Internal diameter	8 875	
	Length	15 6	
	Wall thickness	0 040	
	Reflector		
	Material	Beryllium	
	ID (in)	9 090	
	Thickness (equivalent in)	2 12	
	Height (in)	12 25	
	No fine control drums	2	
	No coarse control drums	2	
	Shield		
	Casing material	SS 321	
	Casing wall thickness (in)	0 060	
	Shield material	LiH	
	Maximum height (in)	25	
	Maximum diameter at base (in)	27 2	
	Minimum diameter at top (in)	20 9	
	Current weight summary (estimated lb)		
	Reactor assembly	170	
	Reflector assembly	117	
	Shield assembly	355	
	Electronic equipment	25	
	Total	667	
III	Performance Characteristics		
	Thermal-Hydraulic		
	Coolant pressure drop (psi)	0 2	
	Maximum fuel temperature (°F)	1336	
	Maximum fuel clad temperature (°F)	1298	
	Average reflector temperature (°F)	770	
	Maximum shield temperature (°F)	1000	
	Minimum shield temperature (°F)	600	
	Nuclear Parameters		
	Average core thermal flux (n/cm^2-sec)	$3\ 4 \times 10^{11}$	
	Mean fission energy (ev)	0 18	
	Average isothermal temperature coefficient (¢/°F)	-0 21	
	Uranium loading (kg U^{235})	4 75	
	Effective delayed neutron fraction	0 008	
	Mean prompt neutron lifetime (μ-sec)	6 5	
	Prepoison reactivity worth ($)	-1 80	
	Initial cold excess reactivity ($)	3 53	
	Lifetime reactivity loss ($)		
	Xenon equilibrium	- 23	
	Samarium burnout	+ 27	
	Temperature and power defect	-2 44	
	Hydrogen loss	- 21	
	Hydrogen redistribution	- 19	
	Burnup and fission product poison	14	
	Total ($)	-2 92	
	Contingency ($)	63	
	Total control drum worth ($)	10 90	
	Total shim worth ($)	1 05	
	1-yr dose at CPU/AGENA mating plane		
	Fast neutrons (nvt)	$1\ 3 \times 10^{12}$	
	Gamma (r/yr)	1×10^7	

1 $ = 0 008 $\Delta k/k$

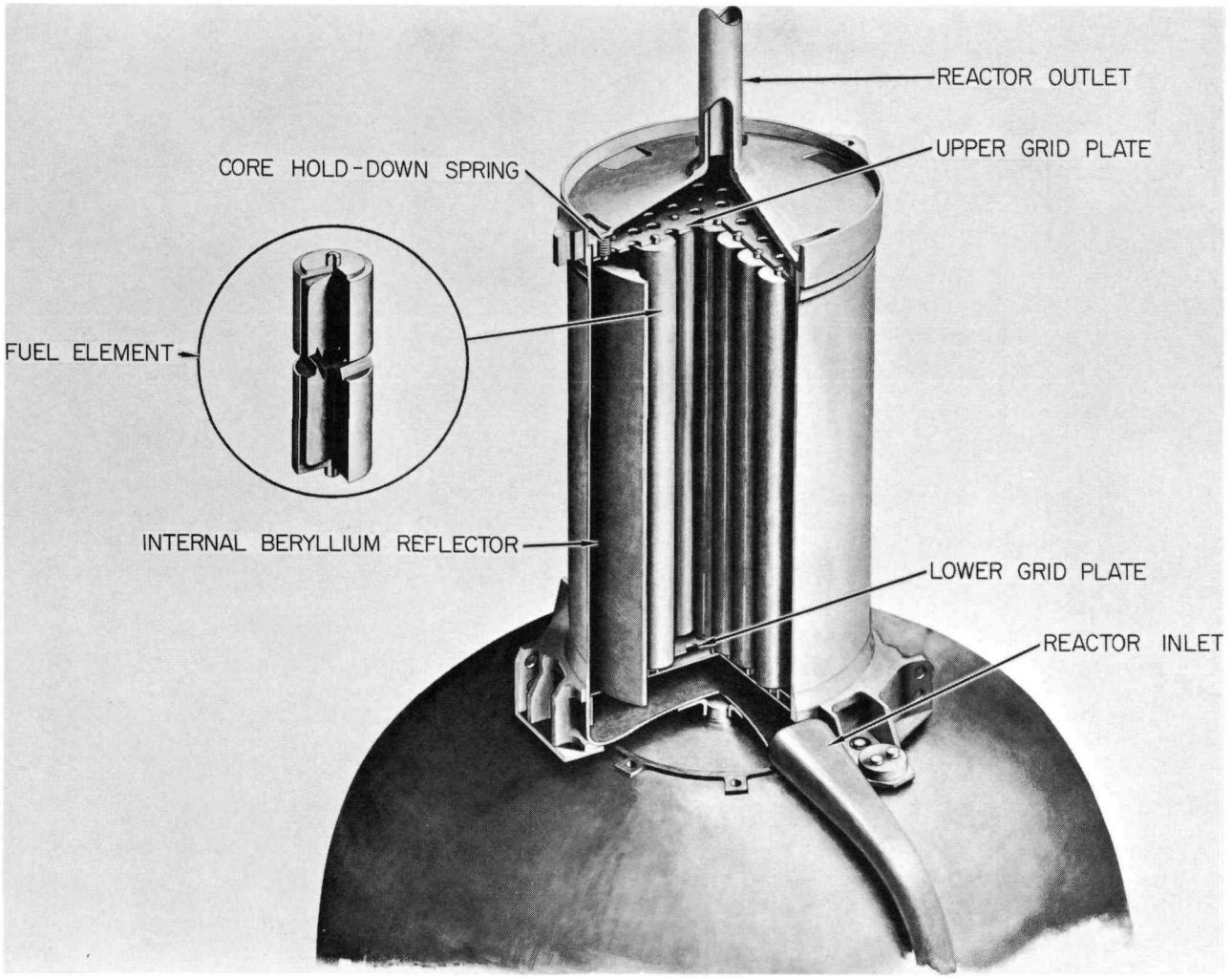

8-1-63 7622-0026

Figure 4. Reactor Assembly, Cutaway View

The fuel-moderator elements contain highly enriched U-235 which is alloyed with zirconium and hydrided to achieve a compact, lightweight core with the desirable control characteristics of a hydrogen moderated reactor. A drawing of a fuel-moderator element assembly is shown on Figure 5. The elements are clad with Hastelloy-N, the inner surface of which is coated with a thin ceramic hydrogen diffusion barrier. The fuel-moderator rod is an alloy of zirconium 10 wt % uranium, hydrided to an N_H of 6.35×10^{22} atoms/cm^3. The nominal, cold radial gap between the rod and the hydrogen barrier is 0.002 in.

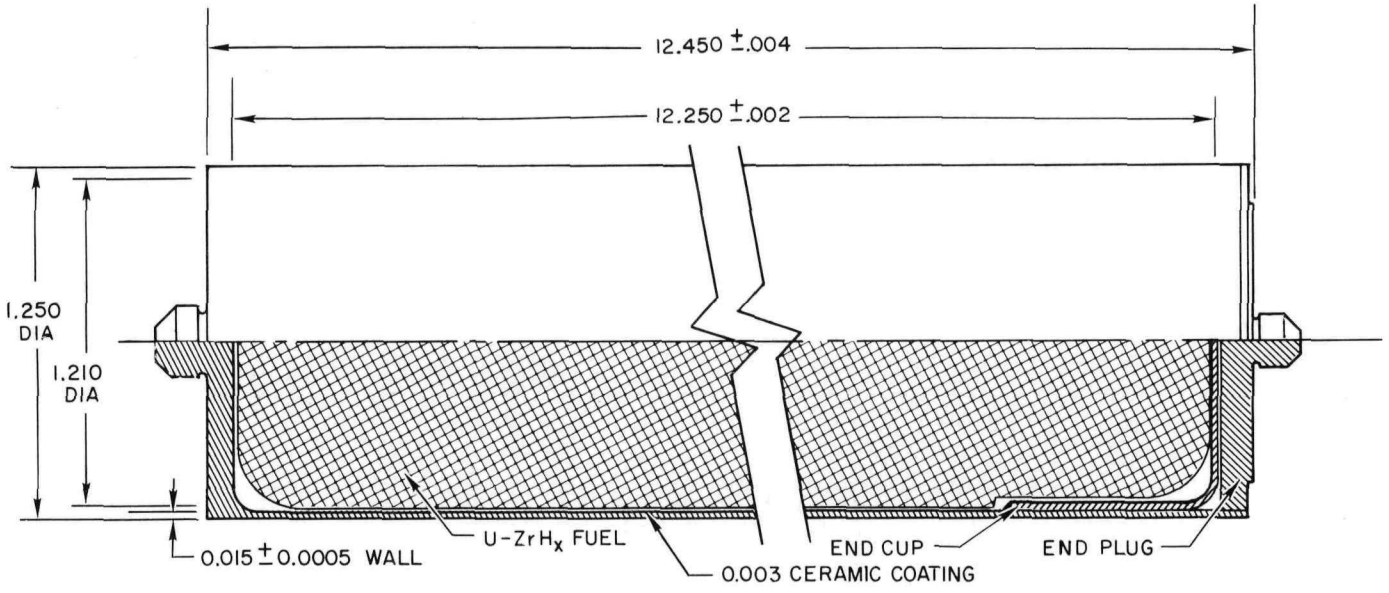

1-10-64 7635-0038

Figure 5. SNAP 2 Fuel Element

The beryllium reflector is mounted external to the reactor vessel and contains four control drums which are rotated to achieve both fine and coarse reactivity control. The reflector is split longitudinally into two halves, hinged at the bottom, and retained at the top with a thin, stainless steel band. Separation of the band, due either to melting upon reentry or actuation of band release devices, permits reflector ejection for reactor shutdown during various phases of launch and orbital operation.

The radiation shield reduces the neutron and gamma dose levels at the Agena mating plane to tolerable levels and also provides structural support for the reactor assembly. The shield consists of a stainless steel casing assembly filled with lithium hydride (LiH) which is cast in place to achieve an efficient, high-temperature structure.

IV. THERMAL-HYDRAULIC ANALYSIS

The thermal-hydraulic analyses described in this section were performed to determine core temperature distributions for a range of power levels and coolant temperatures. Coolant pressure drop across the reactor vessel was also investigated briefly. In predicting the temperature distributions, it was assumed that (1) the coolant flow is maintained proportional to reactor power so as to yield a 200°F coolant temperature rise in the core, (2) the axial and radial power distributions remain constant (neglecting the effect of possible changes in reflector geometry), and (3) the flow is orificed to obtain a (within ±10%) uniform coolant temperature rise in the coolant channels.

Fuel element temperatures were based on the nominal temperature rise in the NaK film, clad, hydrogen barrier material, gas gap and fuel. Peaking factors were included to account for reduced coolant velocity in the cusps of the coolant channel and for the effect of fuel eccentricity inside the clad.

Given the equation for the axial power distribution (Equation 1) and assuming that the reactor core is orificed for equal power-to-flow ratio in all channels, equations can be written as follows to describe the axial temperature distributions in the fuel elements.

$$\frac{\varphi(Z)}{\varphi} = 1.47 \cos (1.479 - 0.2413Z) \qquad \ldots(1)$$

$$(0 \leq Z \leq 12.25 \text{ in.})$$

NaK temperature

$$T_c(Z) = T_{in} + A\left[0.996 - \sin (1.479 - 0.2413Z)\right] \qquad \ldots(2)$$

Hydrogen barrier temperature

$$T_b(Z) = T_c(Z) + BP \cos (1.479 - 0.2413Z) \qquad \ldots(3)$$

Fuel surface temperature

$$T_{fs}(Z) = T_b(Z) + CP \cos (1.479 - 0.2413Z) \qquad \ldots(4)$$

Fuel centerline temperature

$$T_{cl}(Z) = T_{fs}(Z) + DP \cos (1.479 - 0.2413Z) \qquad ...(5)$$

where

T_{in} = reactor inlet temperature (°F)

P = reactor power (kwt)

Z = distance from core inlet (in.)

Because the axial power distribution does not vary with core radius, Equations 2 through 5 may be used for any fuel element, given the proper constants A, B, C, D. The values of these constants for the average and hot fuel elements are given in Table 2.

TABLE 2

CONSTANTS FOR USE IN THE GENERAL EQUATIONS FOR AXIAL POWER DISTRIBUTION CALCULATIONS

	Average Fuel Element	Hot Fuel Element
A	100°F	111°F
B	0.75°F/kw	1.00°F/kw
C	0.29°F/kw	0.38°F/kw
D	0.79°F/kw	1.03°F/kw

Constant A is one-half the NaK temperature rise expected in the channels surrounding the average or hot fuel element. The hot-channel temperature rise has been increased by 10% to account for orifice inaccuracies. The only other quantity that was used to differentiate between the hot and average fuel elements was the radial power factor, which has a value of 1.31.

Equations 3 and 4 permit the evaluation of the circumferential average barrier and fuel surface temperatures at each elevation in the core. Equation 5 permits the evaluation of maximum fuel temperatures located on or near the fuel cylinder centerline. The average fuel temperature at any elevation is closely approximated by the arithmetic average of the fuel surface and the maximum fuel temperature near the fuel centerline.

Figures 6 and 7 show the maximum fuel temperature, maximum fuel surface temperature, and maximum barrier temperature as a function of reactor thermal power for an average fuel element and for the hot fuel element. Figures 8 through 15 show the axial temperature distributions for the average and the hot elements for reactor net power levels of 53, 100, 150, and 200 kwt.

The fuel and barrier temperatures for the average fuel element are used to determine the rate of hydrogen loss from the system. Section V-A of this report describes the use of the temperature information in hydrogen leakage calculations. The hot-element analysis is required to evaluate barrier and cladding integrity. Cladding creep strength is a function of temperature, as discussed in Section V-B. Hydrogen pressure in the annulus between the fuel and the barrier and the growth of fuel during irradiation are also direct functions of fuel temperature. Therefore, the hot-element temperature distribution is used to conservatively estimate fuel element performance capabilities and limitations.

Figure 16 shows the variation of total reactor pressure drop with reactor power. Curves are shown for an orificed and an unorificed core. For both cases, it is assumed that the flow areas of the inlet and outlet nozzles are made proportional to coolant flow. This requires that more than one inlet nozzle be used for power levels above 75 kwt. For the orificed core, it is assumed that the area of the orifice holes is proportional to flow rate, so as to maintain a constant ratio between orifice pressure drop and nozzle pressure drop.

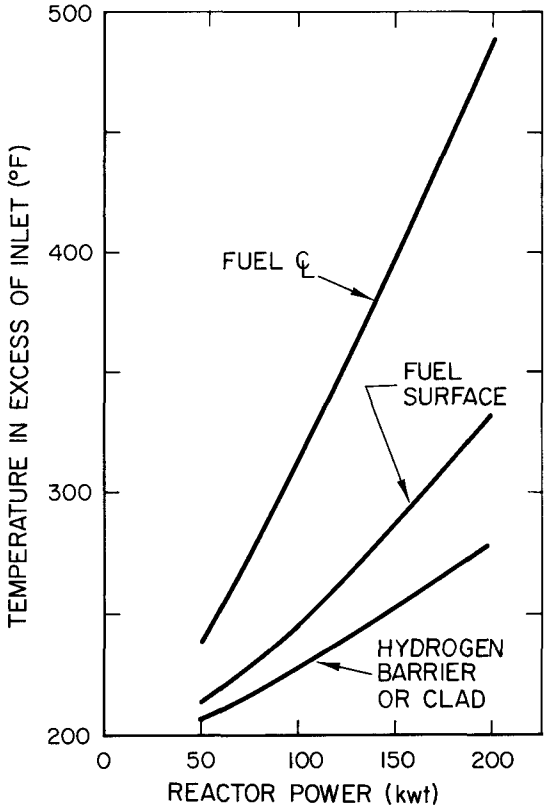

Figure 6. Maximum Fuel ℄ and Clad Temperatures, Average Element

Figure 7. Maximum Fuel ℄ and Clad Temperatures, Hot Element

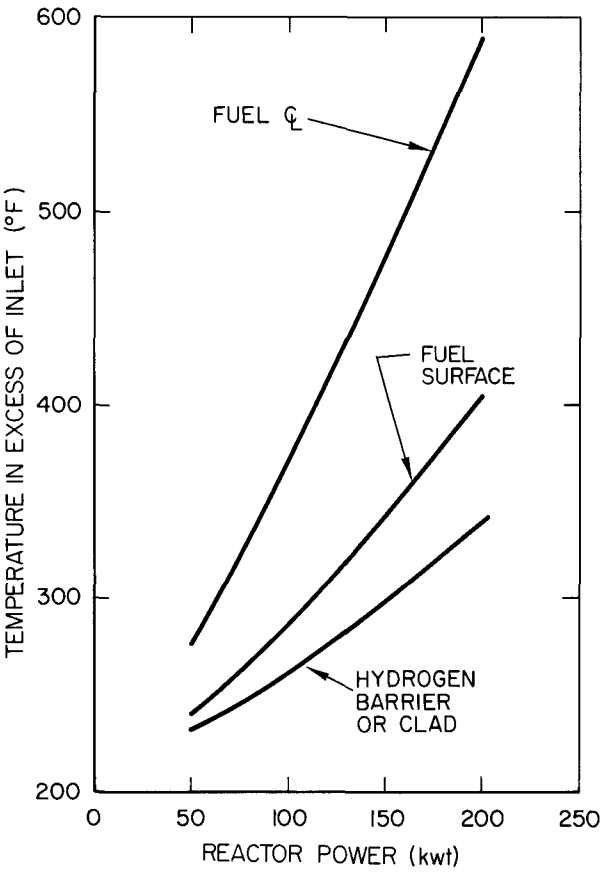

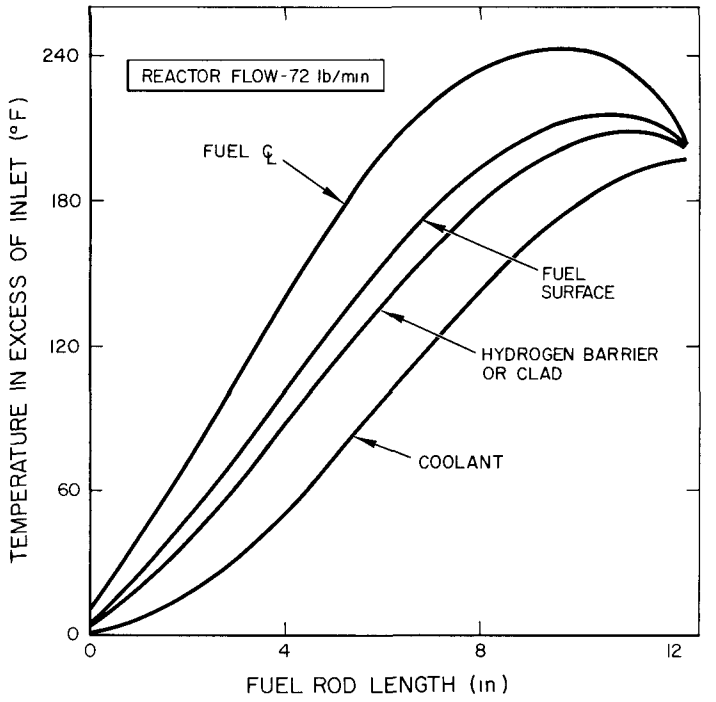

1-22-64 7635-0041

Figure 8. Average Fuel Element Temperature Distribution for 53 kwt Net Reactor Power

Figure 9. Average Fuel Element Temperature Distribution for 100 kwt Net Reactor Power

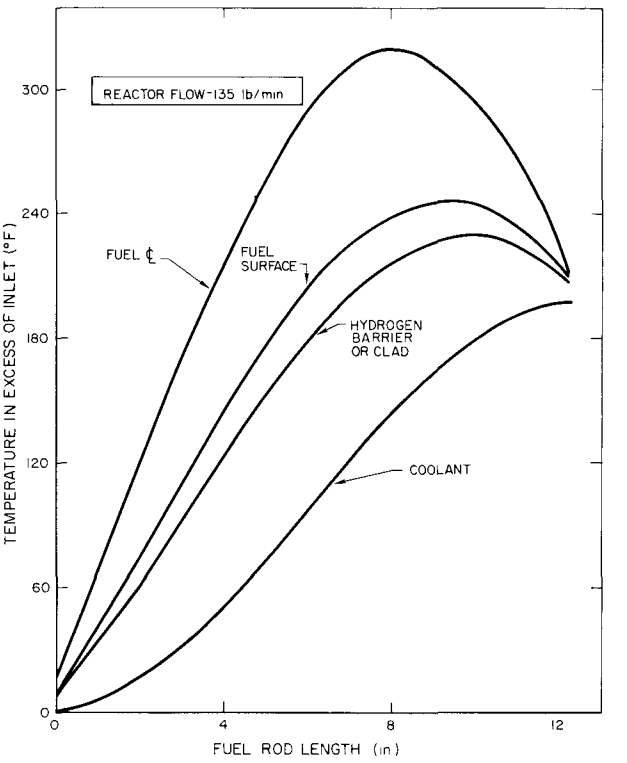

1-22-64 7635-0042

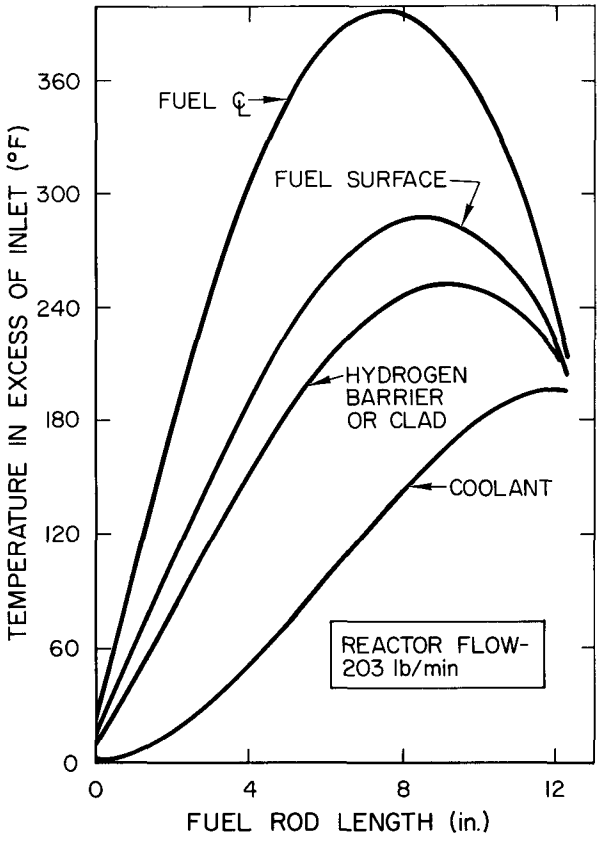

1-22-64 7635-0043

Figure 10. Average Fuel Element Temperature Distribution for 150 kwt Net Reactor Power

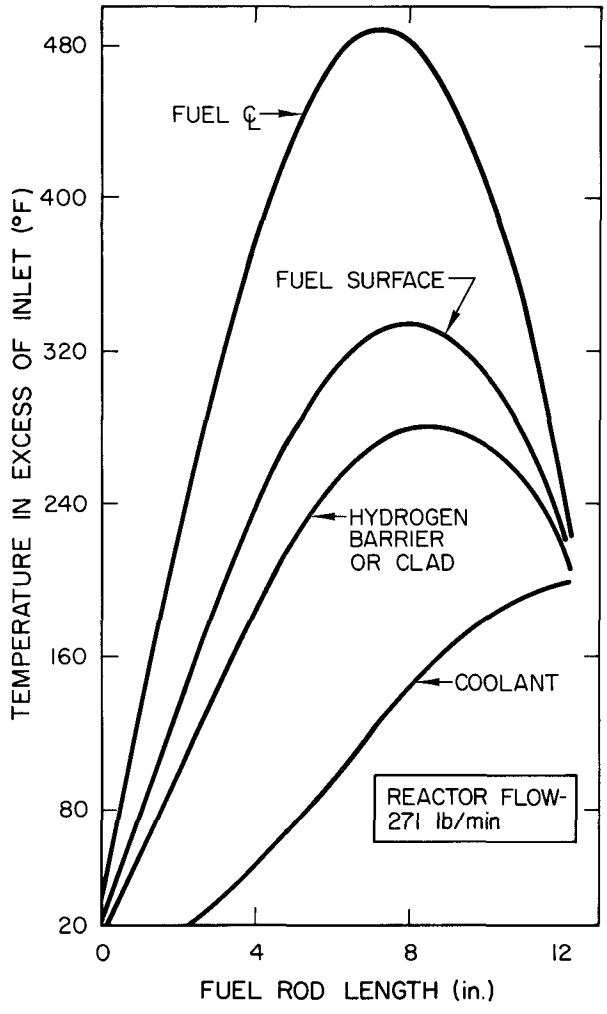

Figure 11. Average Fuel Element Temperature Distribution for 200 kwt Net Reactor Power

1-22-64 7635-0043

Figure 12. Hot Fuel Element Temperature Distribution for 53 kwt Net Reactor Power

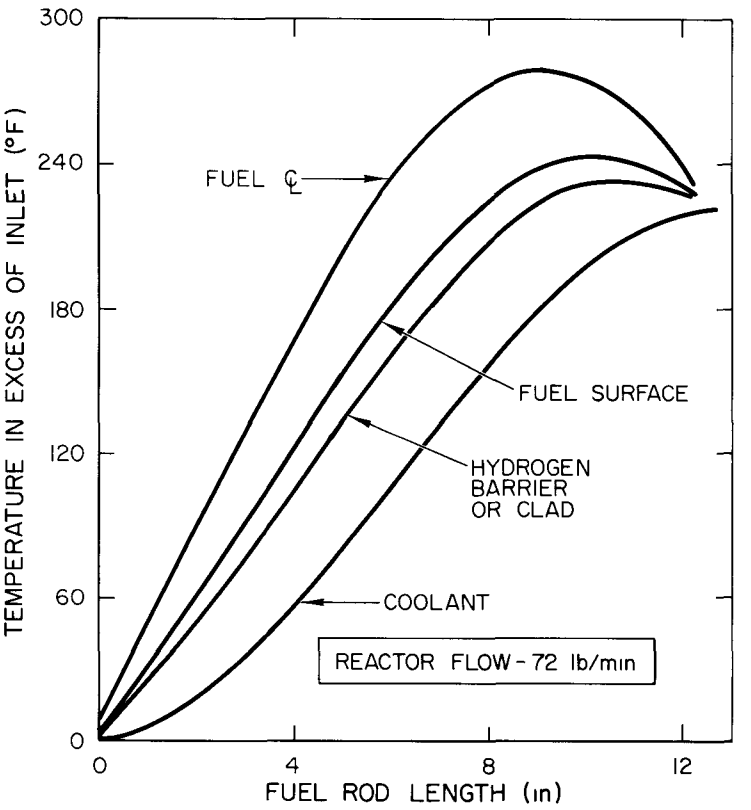

1-22-64 7635-0045

Figure 13. Hot Fuel Element Temperature Distribution for 100 kwt Net Reactor Power

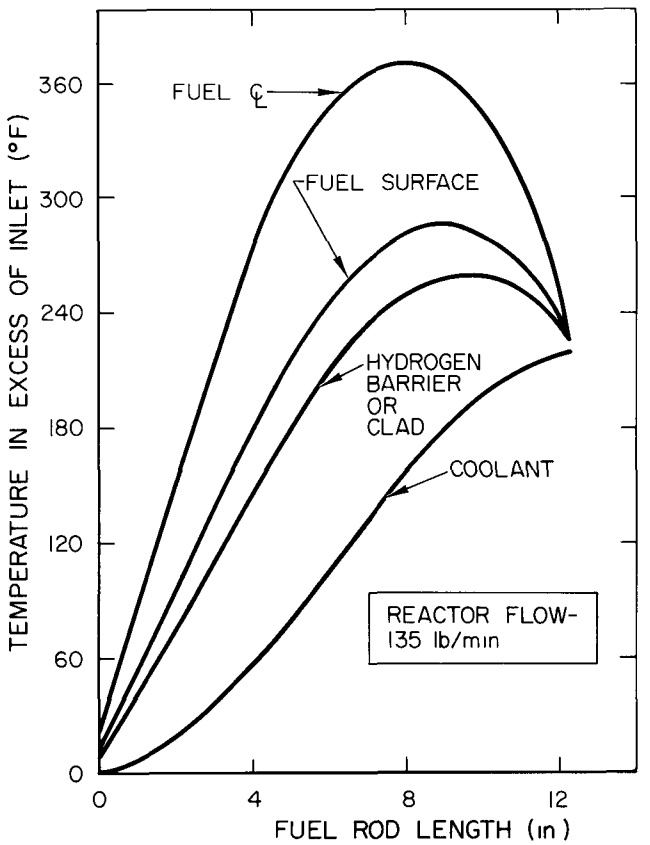

1-22-64 7635-0045

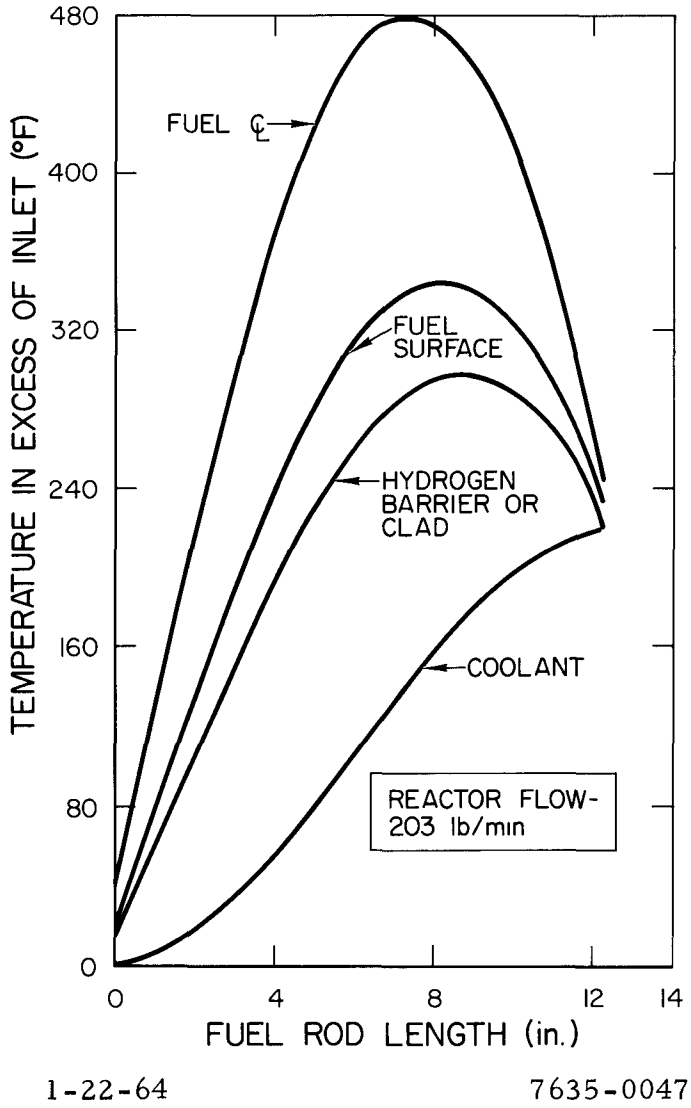

Figure 14. Hot Fuel Element Temperature Distribution for 150 kwt Net Reactor Power

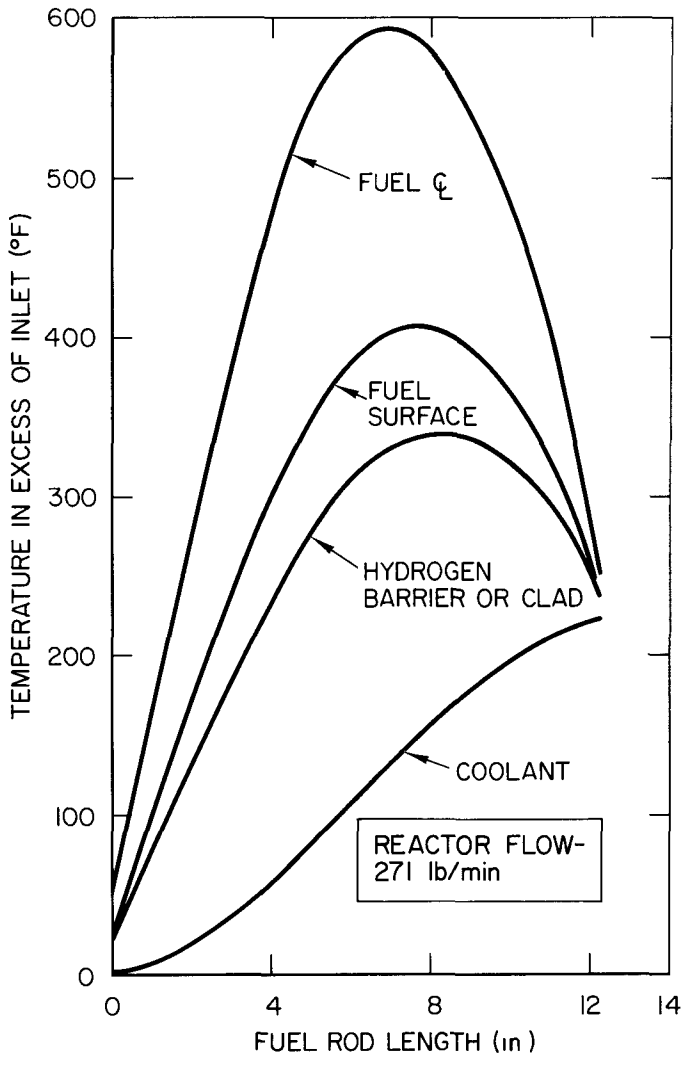

Figure 15. Hot Fuel Element Temperature Distribution for 200 kwt Net Reactor Power

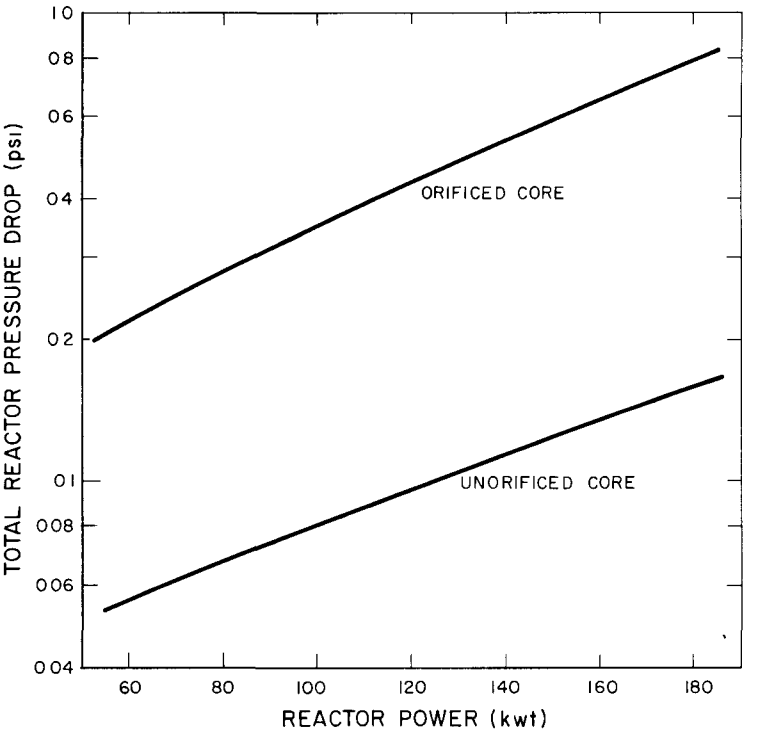

1-21-63 7635-0049

Figure 16. SNAP 2 Reactor Pressure Drop vs Net Reactor Power

BLANK

V. FUEL ELEMENT ANALYSIS

Fuel element performance was evaluated as a function of reactor power and coolant inlet temperature over an initial N_H range of 6.0 to 6.5. The current SNAP 2 Fuel element configuration and carbon content (0.10 wt %) were maintained constant in all cases. The carbon content will be maintained below 10 wt %, consequently, using this value as a constant will result in a conservative estimate of hydrogen leakage. Hydrogen loss rates were computed for the "average" fuel elements, Hastelloy-N cladding strength limitations were determined based upon operation of the "hot" fuel elements (a safety factor of 2 on creep strength was used to account for local "hot spots"), and fuel irradiation swelling was examined. Each of these performance parameters is discussed in detail below.

A. HYDROGEN LEAKAGE

To perform the parametric study, it was necessary to develop a method of estimating fuel element hydrogen loss rates under reactor operating conditions from rates experimentally measured at isothermal conditions. The first step was to assume that the total element permeation was made up of two types of leakage — one through the ceramic coating proper, and the other through defects in the cladding. The blend was considered to be a defect. Previous work had shown that blend permeation could be correlated by an Arrhenius equation (Equation 1) and it was assumed that this equation would hold for defects as well.

$$\varphi_{Bl} = K_{Bl} \sqrt{P}\, e^{-12,760/T} \qquad \ldots(1)$$

where

φ_{Bl} = permeation rate through the blend

K_{Bl} = a constant

P = hydrogen pressure

T = temperature (°R)

Thus φ varies as the square root of the pressure, a characteristic of hydrogen permeation through metals.

Permeation through Solaramic-coated cladding membranes was correlated in a separate study by the Langmuir-type equation:

$$\varphi_{Cl} = \frac{K_{Aging} P T^{5/2} e^{-28,160/T}}{T^{5/2} + 8.432(10)^{13} P e^{-28,160/T}} \quad \ldots(2)$$

where

φ_{Cl} = permeation rate through the cladding proper

K_{Aging} = a second constant

This φ varies almost directly as the pressure, a characteristic of hydrogen permeation through glass.

Adding the two equations gives the total isothermal permeation rate through an element:

$$\varphi_E = K_{Bl} \sqrt{P}\, e^{-12,760/T} + \frac{K_{Aging} P T^{5/2} e^{-28,160/T}}{T^{5/2} + 8.432 \times 10^{13} P e^{-28,160/T}} \quad \ldots(3)$$

where φ_E is permeation rate for whole element. Thus, the isothermal hydrogen loss rate can be expressed as a function of temperature and pressure, providing that the constants are known.

An evaluation was performed for the production lot of 50 fuel elements fabricated for the SNAP 10 FS-1 core to determine proper values for the constants K_{Aging} and K_{Bl} of Equation 3. The evaluation indicated that $K_{Aging} = 1.455 \times 10^6$ and $K_{Bl} = 511.3$, the latter being the average of the sum of the blend and the defect constant for the entire lot of 50 elements. These values of the indicated constants were used to compute permeation rates for the various cases considered in this study.

The dissociation pressure for isothermal fuel hydride is given as a function of temperature and hydrogen concentration by the following equation:

$$P = e^{f_1(H/Zr)\left[e^{-(10^4/T) f_2(H/Zr)}\right]} \quad \ldots(4)$$

where

$$f_1(H/Zr) = -8.8455 + 88.9801(H/Zr) - 78.8961(H/Zr)^2 + 21.3731(H/Zr)^3 \quad \ldots(5)$$

$$f_2(H/Zr) = 12.9720 - 9.7707(H/Zr) + 2.4984(H/Zr)^2 \quad \ldots(6)$$

$$(H/Zr) = \frac{108{,}595\ H}{(100-H)\,(1200-103.22\ C-12U)} \quad \ldots(7)$$

where

H = wt % hydrogen in fuel

U = wt % uranium in fuel alloy prior to hydriding

C = wt % carbon in fuel alloy prior to hydriding

Fuel element operation in a reactor is nonisothermal and, accordingly, hydrogen migrates from high temperature regions to colder temperature regions. When the redistribution of hydrogen is complete, an equilibrium dissociation pressure is obtained which is lower than the dissociation pressure before redistribution. A new computer code designated Hydrogen Redistribution Equilibrium Pressure (HYREP) was written to obtain the equilibrium pressure values used in Equation 3. An axial average fuel temperature profile, expressed as a quadratic in L, is substituted for T in Equation 4. The HYREP computation is based on conservation of hydrogen and the fact that, at equilibrium, $dP_{EQ}/dL = 0$, where EQ is equilibrium.

Figure 17 shows the computed hydrogen equilibrium gradients as a function of initial N_H for a specific case investigated, viz., 100 kw reactor power and 1100°F NaK coolant.

For computation of fuel element permeation in a reactor, i.e., for nonisothermal fuel element operation, integration of Equation 3 is required. It is assumed that equilibrium hydrogen redistribution has occurred and that the distribution of defects in the coating and blend are uniform. Using a total coating area of 49.45 in.^{2} and the specific K_{Aging} and K_{B1} constants presented previously, the indicated integration is:

$$\varphi_E = \frac{511.3\sqrt{P_{EQ}}}{49.45}\int_{A=0}^{A=49.45} e^{-12{,}760/T_{ce}}\,dA + \frac{1.455 \times 10^6 P_{EQ}}{49.45}\int_{A=0}^{A=49.45} \frac{(T_{ce})^{5/2}\, e^{-28{,}160/T_{ce}}}{(T_{ce})^{5/2} + 8.432 \times 10^{13} P_{EQ}\, e^{-28{,}160/T_{ce}}}\,dA \quad \ldots(8)$$

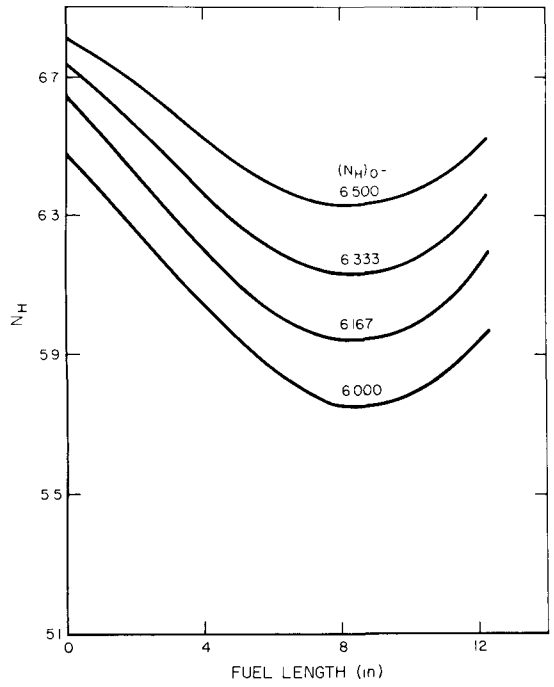

a. Average Axial N_H Gradients for Average Fuel Element

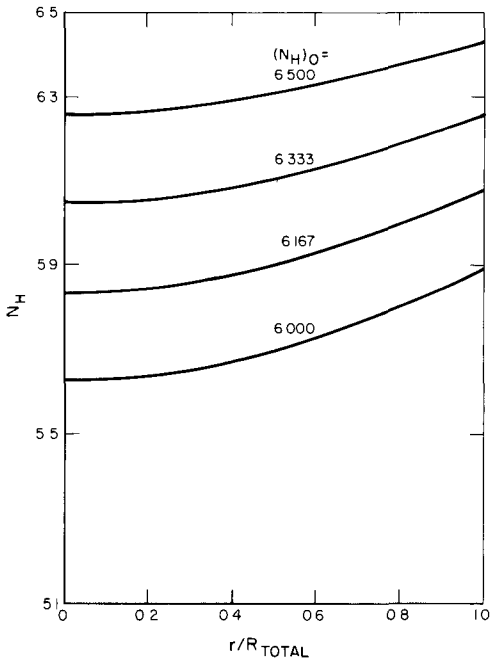

b. Radial N_H Gradients for Average Fuel Element at Peak Fuel Temperature Cross Section

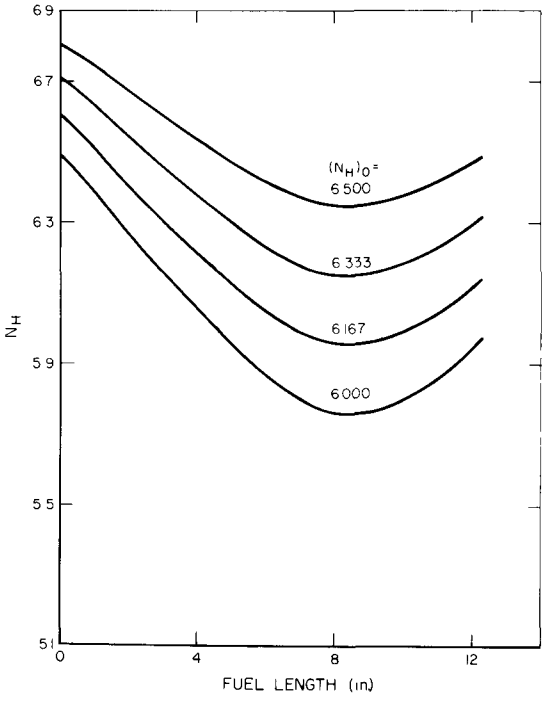

c. Average Axial N_H Gradients for Hot Fuel Element

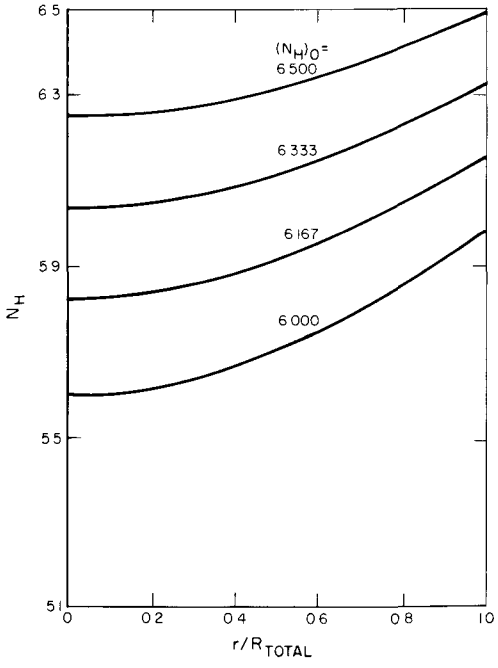

d. Radial N_H Gradients for Hot Fuel Element at Peak Fuel Temperature Cross Section

1-10-64 7635-0050

Figure 17. Fuel Element (0.10 wt % Carbon) Hydrogen Gradients for 100 kw Reactor with 1100°F Coolant Inlet Temperature as Function of Initial Uniform N_H

where

A = cladding area

T_{ce} = cladding temperature (°R)

Solution of Equation 8 was performed numerically using:

$$\varphi_E = 10.34\sqrt{P_{EQ}}\sum_{i=1}^{N}\left[e^{-12,760/(T_{ce})_i}A_i\right] + 2.942 \times 10^4 + P_{EQ}\sum_{i=1}^{N}\left[\frac{(T_{ce})_i^{5/2}\, e^{-28,160/(T_{ce})_i}A_i}{(T_{ce})_i^{5/2} + 8.432 \times 10^{13} P_{EQ}\, e^{-28,160/(T_{ce})_i}}\right] \quad \ldots(9)$$

where

$(T_{ce})_i$ = average cladding temperature (°R)

A_i = the cladding area segment

The results of the hydrogen leakage calculations for the range of parameters studied are presented in Figure 18. As expected, the hydrogen loss rate is a rather sensitive function of initial N_H, coolant temperature, and reactor power level.

In general, the hydrogen loss rates shown in Figure 18 are probably conservatively high for the following reasons: (1) Hydrogen depletion from the fuel over 1-yr of operation was not taken into account in calculating hydrogen loss. The fuel was assumed to remain at its initial hydrogen concentration throughout the reactor lifetime. With this assumption, hydrogen loss is overestimated by as much as 50% in the higher temperature, higher power cases; (2) Recent S8ER experimental information indicates that use of the general methods and constants discussed above, with allowance for hydrogen depletion, still tends to overestimate observed in-pile hydrogen loss rates by as much as 100%. The hydrogen loss information contained in Figure 18 therefore appears to contain a safety factor of approximately 2, which allows for uncertainties in loss due to hot spots, locally high hydrogen or additive concentrations.

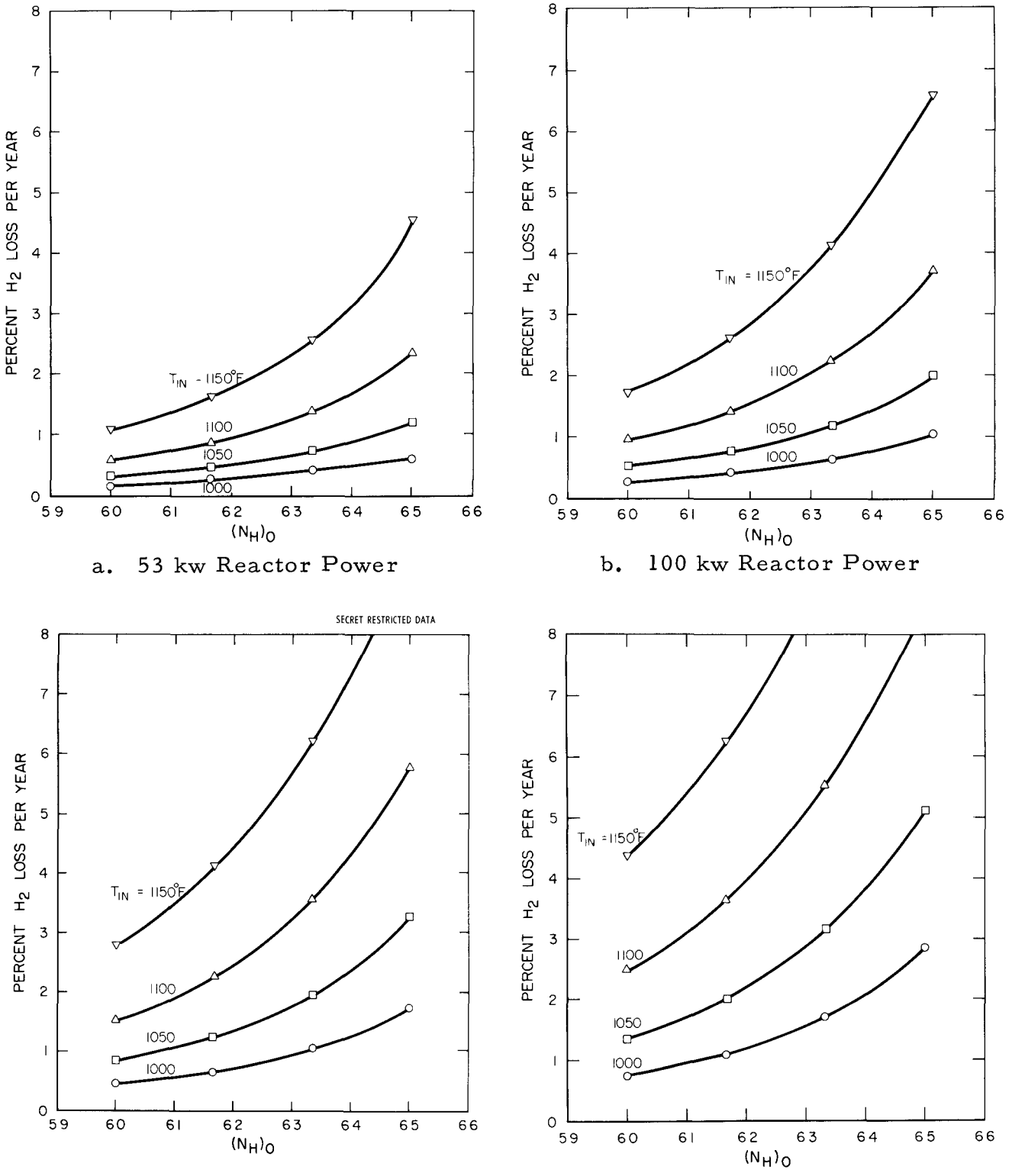

Figure 18. Hydrogen Loss Rates for Average Fuel Elements (0.10 wt % Carbon) for Various Reactor Powers as Function of NaK Coolant Inlet Temperatures

B. CLADDING STRENGTH

It can be shown that long term creep is the limiting criterion for evaluation of Hastelloy-N cladding strength. A strain limit of 0.2% in 10,000 hr was used in this study because laboratory testing has shown that the ceramic coating is still effective as a hydrogen barrier at this strain level. ORNL creep data for Hastelloy-N may be correlated by the following equation:

$$\sigma = 5.57\left(\frac{t}{\epsilon}\right)^{-0.202} e^{17,700/T} \qquad \ldots(10)$$

where σ = creep strength (psi).

Because of the unknown effects of irradiation of Hastelloy-N, it is considered desirable to use a safety factor of 2.0 with Equation 10 in computing the allowable stress, viz:

$$\sigma = 2.785\left(\frac{t}{\epsilon}\right)^{-0.202} e^{17,700/T} \qquad \ldots(11)$$

which, for 10,000 hr life and an allowable strain of 0.2%, reduces to:

$$\sigma = 0.312\, e^{17,700/T} \qquad \ldots(12)$$

Equation 12 was used to compute the limiting cladding stress, with T set equal to the peak cladding temperature in degrees Rankine.

Using the basic hoop stress equation for thin wall pressure vessels, viz:

$$\sigma = \frac{PD}{2x_w} \qquad \ldots(13)$$

and assuming a NaK coolant pressure of 20 psia, the following equation gives the resultant cladding stress:

$$\sigma = \frac{\left[(P_{EQ})(14.7) - 20\right] D}{2x_w} \qquad \ldots(14)$$

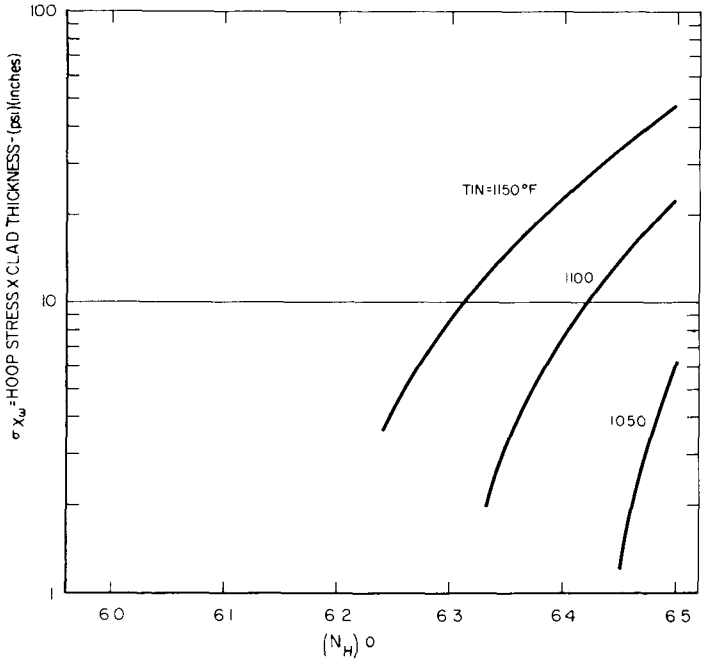

a. 53 kw Power Level

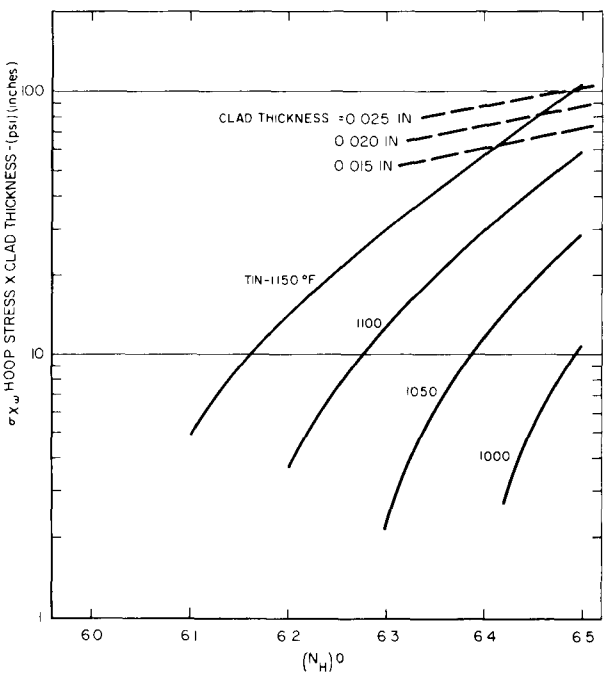

b. 100 kw Power Level

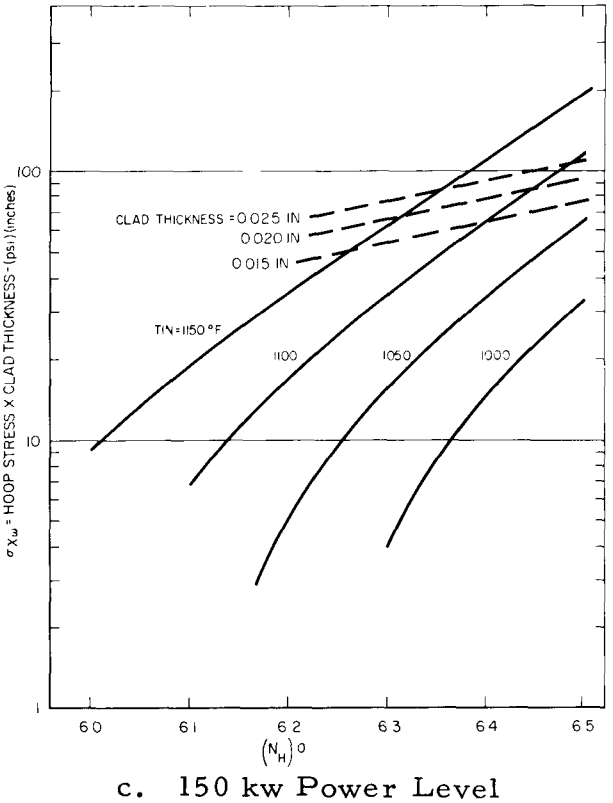

c. 150 kw Power Level

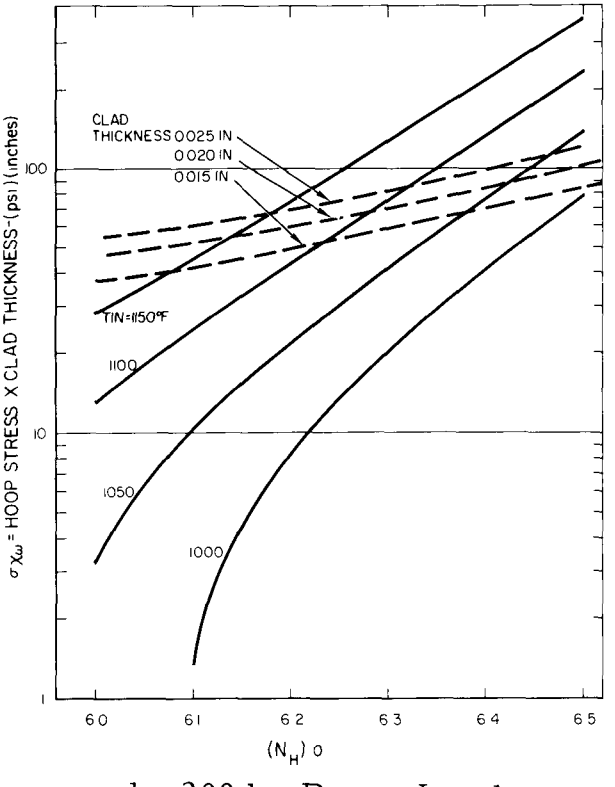

d. 200 kw Power Level

1-10-64

7635-0052

Figure 19. Hot Fuel Element (0.10 wt % Carbon) 10,000-hr Hastelloy-N Cladding Creep Strength Evaluations for Various Reactor Powers as Function of NaK Coolant Inlet Temperatures

where

P = internal pressure (psi)

D = tube diameter

x_w = tube wall thickness

Equation 14 permits calculation of the actual cladding stress, using the equilibrium hydrogen dissociation pressure.

Figure 19 shows the calculated clad stresses and creep limits for various pow power levels, coolant temperatures, and cladding thicknesses. In all cases the calculated stress is based on nominal values of cladding thickness, N_H, carbon addition, etc. From the curves given in Figure 19 it can be seen that with an N_H of 6.35 or less and an inlet temperature of 100°F, that only in the 200 kw case is the structural integrity of the cladding questionable.

C. FUEL GROWTH DUE TO IRRADIATION

The following equation was used to compute change in fuel volume as a function of metal atom percent burnup and peak fuel temperature (°R):

$$\frac{\Delta V}{V}\% = 3770\, b^{1.5}\, e^{-12{,}000/T} \qquad \ldots(15)$$

where

V = volume

b = burnup (total metal atom percent)

T = temperature (°R)

The fuel element, excluding end hardware, was considered to be composed of six 2-in. increments rather than a single 12-in. rod. The radiation-induced swelling in each increment was determined. This volume increase was assumed to be isotropic and dimensional changes for each increment were calculated. Only the increment having the highest temperature and burnup was considered in determining the radial change; the incremental axial changes were summed to obtain the total axial change. To determine the available volume, the differential thermal expansion between the fuel and the cladding was calculated for each 2-in. increment, using the average temperature in each component. The resultant clearance was then computed. Summation of the axial changes is again required. Comparing the radiation-induced dimensional changes with the available clearance, mechanical interference exists when the change due to swelling exceeds the clearance.

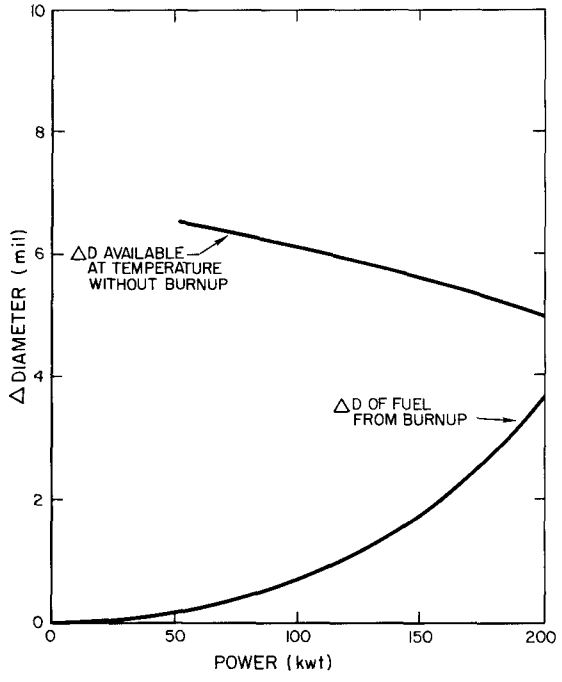

1-22-64 7635-0053

Figure 20. Diametral Clearance vs Reactor Power for 53 kwt Reactor Fuel Element

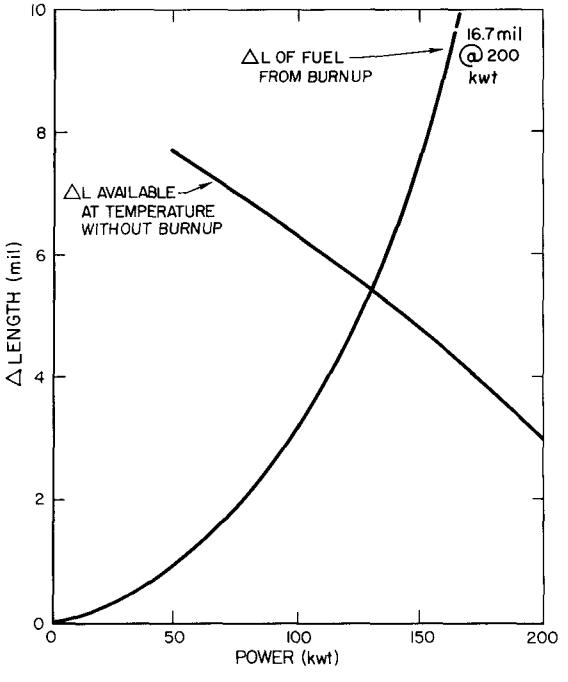

1-22-64 7635-0054

Figure 21. Axial Clearance vs Reactor Power for 53 kwt Reactor Fuel Element

The calculated dimensional changes and available clearances are plotted in Figures 20 and 21 for the reactor powers of interest. Referring to Figure 20, no mechanical interference is shown in the radial direction for any reactor power considered. Figure 21 shows interference beginning in the axial direction below a reactor power of 150 kwt. It is estimated that a 15-mil reduction in the length of the fuel rod will eliminate the axial interference for all cases up to a reactor power of 200 kwt. Therefore, it is concluded that, with a slight reduction in fuel rod length, the reference fuel element design for the SNAP 2 reactor, up to and including reactor powers of 200 kwt, is not limited from the standpoint of mechanical interference caused by fuel swelling.

Equation 15 was derived empirically from the results of earlier irradiations of small SNAP fuel specimens in a limited temperature and burnup range. Later preliminary data, from hot cell examinations now underway, indicate that the volume changes are no greater than those which are predicted by this relationship. Confirmation of the burnups of the later specimens is required for a final evaluation. The latest specimens are also small and further irradiations

of larger prototype fuel elements must be completed before adequate predictions of fuel element performance in an irradiation environment can be made. However, there appears to be little question that Equation 15 predicts fuel swelling behavior that is conservative from the design standpoint.

This study assumed that the criterion for an allowable limit on fuel swelling was mechanical interference between the fuel and the hydrogen barrier. No allowance was made for cladding creep in this part of the study. Equation 15 was used to compute the fuel swelling resulting from operation at various reactor power levels; the volume available in the fuel element to accommodate swelling was calculated from differential thermal expansion considerations. The nominal dimensions of the fuel element for the 53 kwt reactor were used in computing the available volume. For each reactor case (53, 100, 150, and 200 kwt), the temperature and burnup conditions of the hottest fuel element in the core were chosen. In all cases, a 200°F $\Delta\Gamma$ and a coolant outlet temperature of 1300°F were assumed.

BLANK

VI. NUCLEAR ANALYSIS

Nuclear limitations on the temperature and power levels attainable in the SNAP 2 core arise because of increased reactivity losses associated with operation at these levels. The eight modes of reactivity change associated with a SNAP 2 core are (1) temperature defect, (2) power defect, (3) xenon buildup, (4) hydrogen redistribution, (5) fuel depletion, (6) fission product buildup, (7) hydrogen leakage, and (8) samarium burnout and buildup. To a first approximation, temperature defect is dependent upon temperature only; power defect, xenon buildup, hydrogen redistribution, fuel depletion, fission product buildup, and samarium effects are dependent upon power level only; hydrogen leakage is a strong function of temperature, power, and hydrogen concentration. A more detailed description of the dependence of these effects on power and temperature is given below.

A. ISOTHERMAL TEMPERATURE DEFECT

This defect in a SNAP 2 reactor is due mainly to contributions from grid plate expansion, and spectrum changes. The grid plate expands radially, decreasing the density of materials in the core and increasing neutron leakage, the axial expansion of the fuel also increases the core size, decreasing densities and increasing leakage. Increased temperatures harden the neutron spectrum in the core, decreasing neutron cross sections and thereby further increasing leakage. In SNAP 2 nuclear analysis, isothermal temperature defects are calculated by correcting S2DR experimental temperature coefficients for the fact that Carpenter LE-42 (Invar) rather than Hastelloy-C is the grid plate material. The resulting isothermal temperature defects used are listed below:

Average Temperature (°F)	SNAP 2 Temperature Defect ($)
1100	2.21
1150	2.35
1200	2.49
1250	2.64

B. POWER DEFECT

The power defect in a SNAP 2 reactor arises from the fact that the core is not isothermal during power generation. The effects of distributed temperature in the core are lumped into a power coefficient. A value of 0.42¢/kw[1] was used in this study.

C. XENON BUILDUP REACTIVITY

This effect was calculated from a combined analytical and experimental method. The steady state xenon concentration was calculated at various powers from the standard xenon buildup equations. The worth of the xenon was assumed to be linear with xenon concentration and was normalized to an experimental value of 13.4¢ at 30.5 kwt as measured in S2DR.

D. HYDROGEN REDISTRIBUTION REACTIVITY LOSS

This loss arises from the migration of hydrogen from the hotter to colder regions of the fuel elements under the influence of a temperature gradient. Since the colder regions are also regions of less nuclear importance, a net reactivity loss results. The loss was calculated by the HYTRAN code. S2-DR experimental information has shown that the magnitude of the reactivity defect accompanying hydrogen redistribution is predicted relatively accurately by HYTRAN. There are also experimental indications that the code tends to overestimate the rate of hydrogen redistribution. However, exact knowledge of the rate of hydrogen redistribution is not required in design of actively-controlled reactors. The results are shown in Figure 22.

E. FISSION PRODUCT BUILDUP REACTIVITY LOSS

This loss was estimated from ORNL data.[2] Fuel depletion losses were calculated with the AIM-6 code.[3] Results are shown in Figure 23.

F. HYDROGEN LEAKAGE RATES

The hydrogen leakage rates through the cladding were calculated as a function of temperatures and power taken from the correlation of Nathan.[4] These leakage rates were converted into reactivity by means of a constant hydrogen worth of 64¢/% change in hydrogen. Results are shown in Figures 24 and 25.

G. SAMARIUM CONCENTRATIONS

Samarium concentrations as functions of power and time were calculated using standard differential equations for this phenomenon, the reactivity effect of a particular samarium concentration was obtained using the AIM-6 code. Calculations were based on a constant samarium loading of 8.0 mg Sm_2O_3/in. of active fuel length. Uncertainties in samarium loading and samarium reactivity worth were not considered, since minor effects of this nature can be corrected by control drum movement in an actively-controlled system.

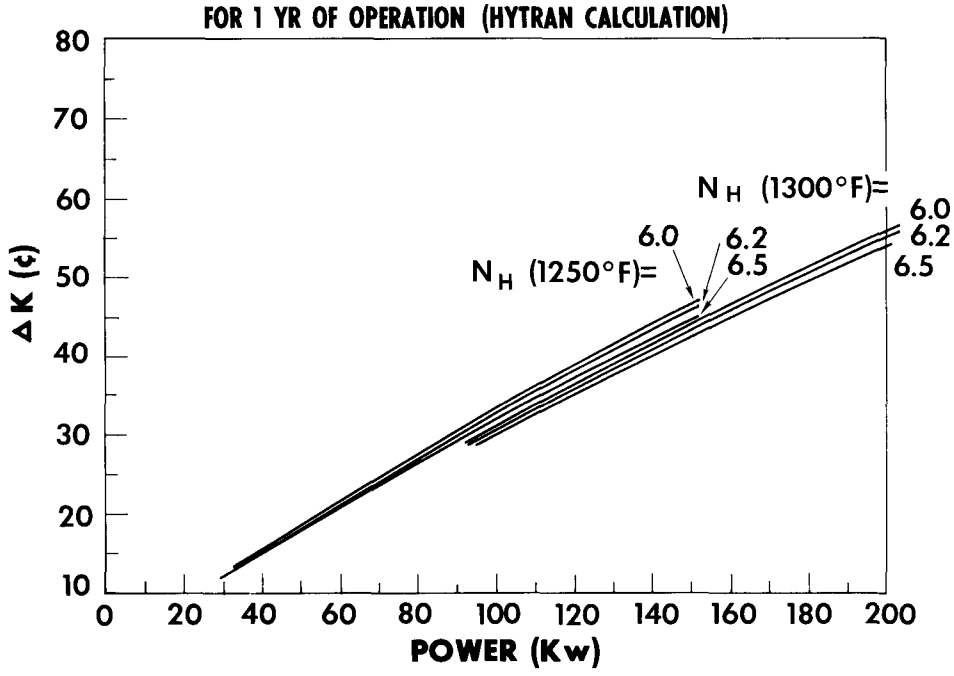

10-9-63 7622-0071

Figure 22. Steady State Reactivity Loss Due to H_2 Distribution vs Power

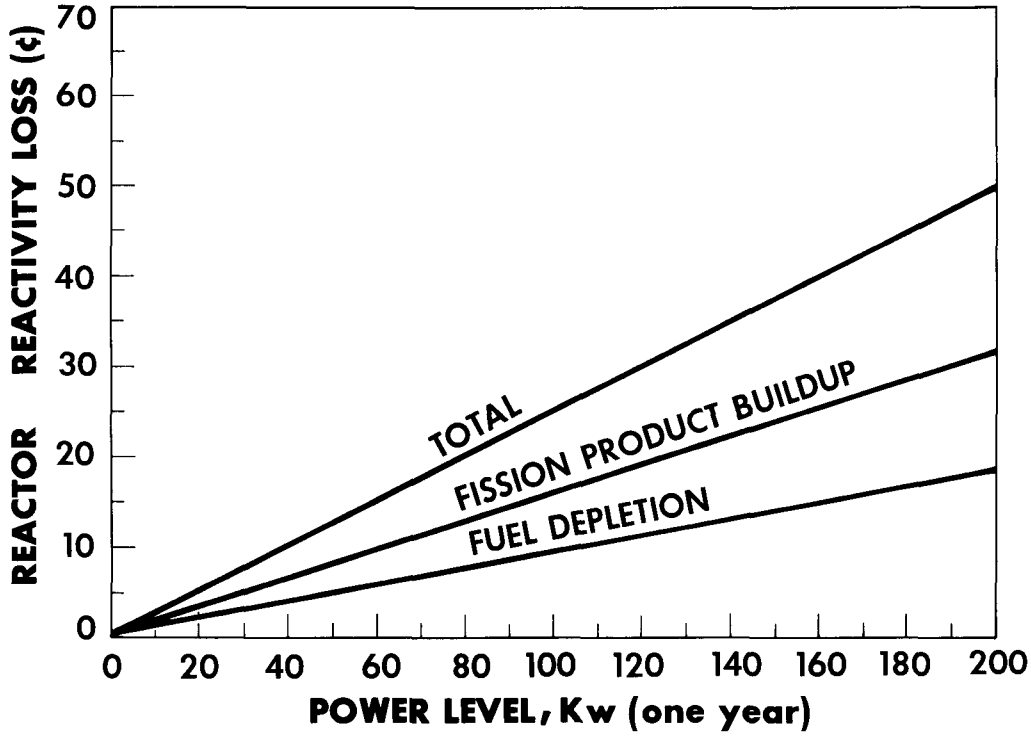

10-9-63 7622-0072

Figure 23. Fission Product Buildup and Fuel Depletion Reactivity Loss for One Year Operation

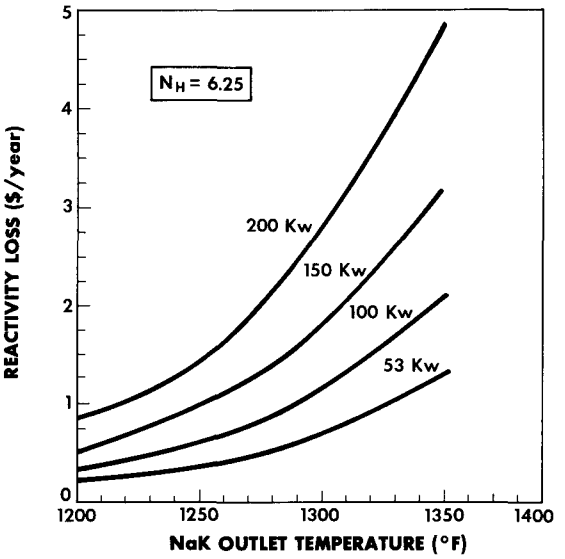

10-9-63 7622-0079-1

Figure 24. Reactivity Loss Rate Due to Hydrogen Leakage, N_H = 6.25

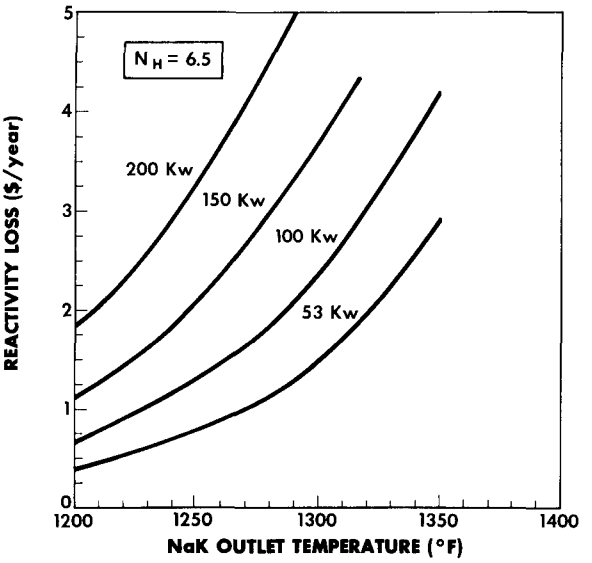

10-8-63 7622-0079

Figure 25. Reactivity Loss Rate Due to Hydrogen Leakage, N_H = 6.5

Reactivity requirements for one year operation at a particular power and temperature were then calculated as the sum of the above eight effects described above. Some examples of reactivity requirements are shown in Table III.

TABLE 3

REACTIVITY REQUIREMENTS

POWER (kw)	55	200	150
NaK OUTLET TEMPERATURE (°F)	1200	1200	1300
TEMPERATURE AND POWER DEFECT	$ 2.44	$ 2.63	$ 2.91
XENON BUILDUP	.23	.75	.59
HYDROGEN REDISTRIBUTION	.19	.61	.43
FISSION PRODUCT BUILDUP	.09	.31	.24
FUEL DEPLETION	.05	.18	.14
Sm BURNOUT*	-.27	-.56	-.51
HYDROGEN LEAKAGE	.21	.84	1.74
TOTAL (reactivity loss for 1 yr.)	$2.92	$4.76	$5.54

*Sm BURNOUT LEADS TO A REACTIVITY GAIN. THE PRESENT SINGLY-SHIMMED SNAP 2A CORE HYDRIDED TO N_H= 6.25 HAS A COLD EXCESS REACTIVITY OF $ 3.58 THE ADDITION OF 20 POUNDS OF BERYLLIUM TO THE REFLECTOR RAISES THE COLD EXCESS REACTIVITY TO $ 5.56

Available absolute excess reactivities were calculated by correcting SCA-4C experimental results for differences in hydrogen level, samarium loading, grid plate material, and reflector-core gap thickness. The resulting excess reactivity was $3.19 for a cold, Sm-poisoned, unshimmed SNAP 2 core at an N_H level of 6.25.

High power and temperature operation requires higher initial excess reactivities; either the thickness of the beryllium reflector or the hydrogen level of the core had to be increased. From a weight penalty point-of-view, the most effective method for reactivity increase is increase in hydrogen content. Because of the use of two coarse control drums which are snapped in by springs and due to ground handling safety considerations, there is a cold shutdown margin requirement of 50¢ with two drums in, which cannot be maintained

as the hydrogen level is increased at constant reflector thickness. In order to maintain the shutdown margin with initial higher excess reactivities, the increased reactivity requirement must be built in by increasing the beryllium reflector thickness at constant or even decreased hydrogen concentrations. This helps to increase shutdown margin due to higher control drum worth. This effect is illustrated in Figure 26. If an excess reactivity of $5.00 is needed for a particular mission, it can be obtained at an N_H of 6.5 and a beryllium thickness of 2.23 in. This configuration has a 2-drum shutdown margin of only about 15¢ however, and is unsatisfactory for safety reasons. The same excess reactivity can be obtained at an N_H of 6.25 and a beryllium thickness of 2.95 in. The shutdown margin of this configuration is about 60¢ which is satisfactory.

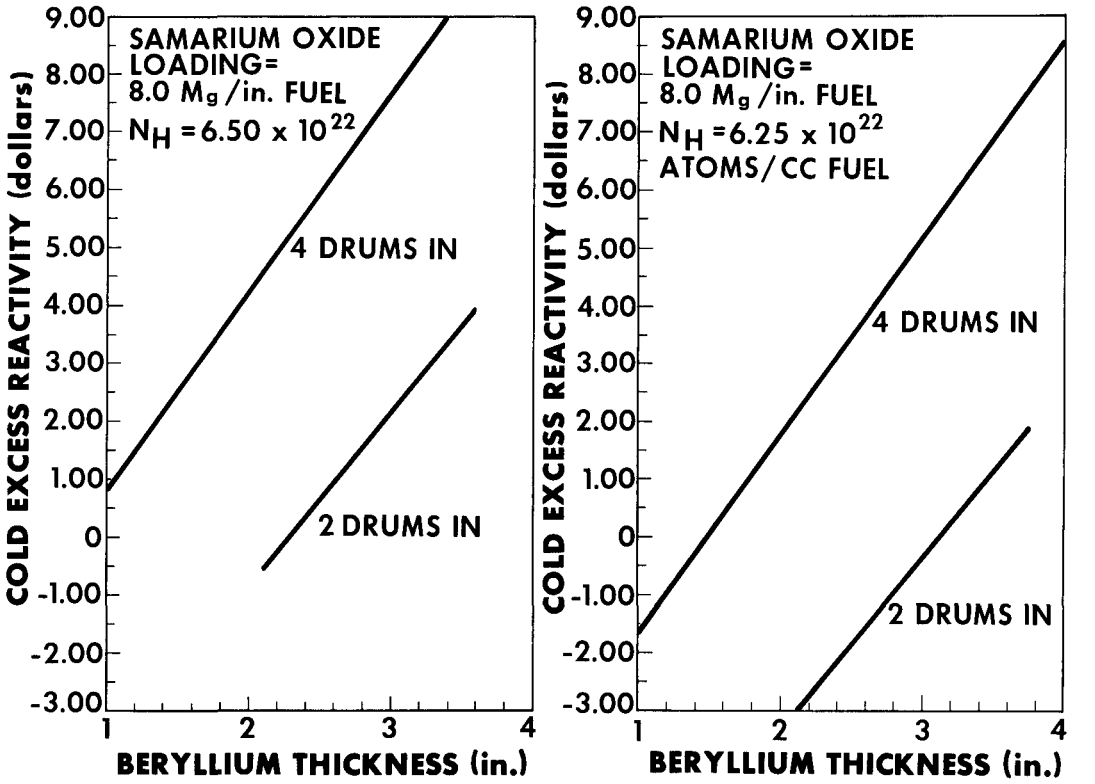

10-8-63 7622-0070

Figure 26. Cold Excess Reactivity of SNAP 2 Core

An optimization study was made to determine the highest N_H level which could be tolerated while still maintaining a sufficient shutdown margin with the present prepoison loading. Figures 27 and 28 show the resulting optimum N_H level and resulting weight penalties for various power-temperature operation.

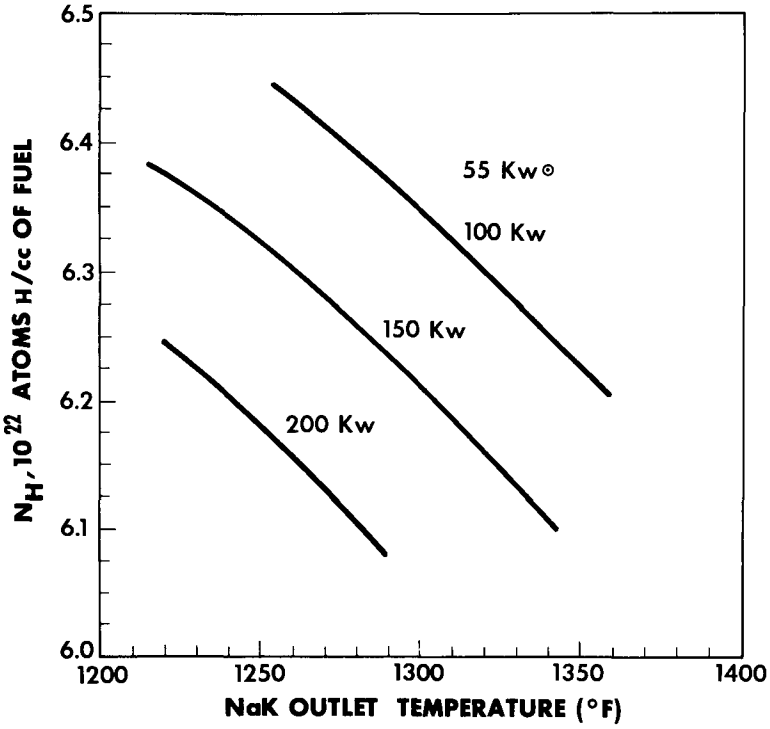

10-7-63 7622-0068

Figure 27. Optimum Hydrogen Level

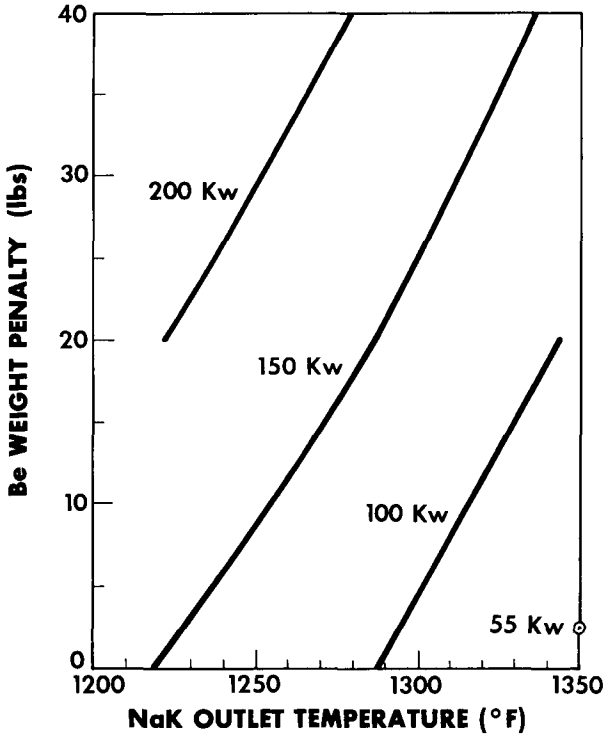

10-7-63 7622-0067

Figure 28. Be Weight Penalty vs NaK Outlet Temperature

Figure 1, which was shown in Section II, illustrates the power and temperature limitations for various beryllium weight penalties.

In addition, there is a shield weight penalty associated with operation at advanced performance conditions. This arises both from the additional shield length required to attenuate the increased radiation associated with higher power operation and from the increased shield radius necessary to shadow the greater thickness of beryllium associated with high power and/or temperature operation. The reflector plus shield weight penalty is shown in Figure 2, Section II.

A major limiting assumption in the study was that of constant samarium prepoisoning. Calculations were based on a samarium prepoison level of 8.0 mg Sm_2O_3/in. of active fuel length in order to reduce the number of cases to be studied. Subsequent calculations have shown that increases in prepoisoning would increase the cold shutdown margin or allow higher hydrogen levels for a given shutdown margin requirement. These higher hydrogen levels would in turn require a smaller beryllium weight penalty for a given set of operating conditions. Use of a poison with a higher cross section, such as gadolinium, would also lead to increased performance due to more complete prepoison burnout over the 1 yr operating lifetime of the reactor.

The main uncertainties in the study arise through uncertainities in hydrogen leakage, weights, and worths of particular reflector configurations. The hydrogen loss information used was based upon "average" elements (defined as an element producing 1/37 of the core power) and averaged hydrogen worths. Distributed temperature effects and distributed hydrogen worths will increase the hydrogen leakage reactivity losses. Another major uncertainty associated with use of hydrogen loss information from Reference 4 is the assumption that in-pile barrier performance at advanced SNAP 2 temperature can be predicted on the basis of out-of-pile isothermal permeation tests conducted at 1200°F. However, recent S8ER experimental information indicates that use of the hydrogen loss equations and constants discussed in this report tends to overestimate observed in-pile hydrogen loss rates by as much as 100%. Thus the hydrogen loss rates quoted, though uncertain, should be conservative.

Reflector worths were calculated by homogenizing the mass of beryllium in the reflector into an equivalent volume annulus. Since present reflector designs provide more beryllium near the center plane of the reactor, which is

a region of higher worth, this homogenization underestimate the reactivity worth of added beryllium. On this basis, the study maintained the approach of obtaining conservative results. The SCA-4A reflector worth experiments will provide information regarding distributed beryllium worths and will decrease this calculational uncertainty.

Although these uncertainties exist in the calculation, it is felt that the trends shown by the results are real, although the actual numbers shown may be changed as further experimental and operational information become available. Significant increases in power level and/or temperature over the reference SNAP 2 values of 53 kwt at 1200° F NaK outlet have been shown to be attainable with only minor reflector redesign.

REFERENCES

1. J. Miller, R. L. Brehm, and W. J. Roberts, "Temperature Coefficients and Spectra in the Hydride Moderated SNAP Reactors," NAA-SR-7140, 1962.

2. J. O. Blomeke and Mary F. Todd, "Uranium-235 Fission Product Production as a Function of Thermal Neutron Flux, Irradiation Time, and Decay Time," ORNL-2127.

3. H. P. Flatt and D. C. Baller, "The AIM-6 Code, NAA Program Description," January 1961 (internal document).

4. M. E. Nathan, "Fuel Element Parametric Study.....Advanced SNAP 2 Reactor," NAA-SR-MEMO-8520-Addendum I (Secret), June 1963.